NASA
Technical
Paper
2217

April 1984

Study of Stator-Vane Fluctuating Pressures in a Turbofan Engine for Static and Flight Tests

Arnold W. Mueller

NASA

Study of Stator-Vane Fluctuating Pressures in a Turbofan Engine for Static and Flight Tests

Arnold W. Mueller

Langley Research Center
Hampton, Virginia

SUMMARY

As part of a program to study the fan noise generated from turbofan engines,
fluctuating surface pressures induced by fan-rotor wakes were measured on core- and
bypass-stator outlet guide vanes of a modified stator assembly of a JT15D-1 engine.
Tests were conducted with the engine operating without an inflow control device on an
outdoor test stand and in flight while mounted beneath the wing of a test-bed air-
craft. Results of data analyses show that as the aerodynamic wakes shed from the
rotor changed amplitude and shape with engine speed, the surface pressures on the
stator vanes exhibited the effect of wake changes. Both core and bypass vanes had a
nonuniform spanwise distribution of narrow-band fluctuating pressure at blade-passage
frequencies with high coherence between measurement locations. Pressures measured at
fan-rotor blade-passage frequencies were generally higher for static conditions than
for flight. A study of the random characteristics of these amplitudes indicated that
the tone amplitudes were less stable under static conditions than in flight. As the
engine speed increased during both static and flight tests, the core amplitudes gen-
erally became less dominated by noise and the bypass amplitudes became more dominated
by noise. Fluctuating pressures measured at the blade-passage frequency of the high-
speed core compressor were interpreted to be acoustic; however, disturbance trace
velocities for either the convected rotor wakes or acoustic pressures were difficult
to interpret because of the complex environment.

INTRODUCTION

Noise research on high-bypass-ratio turbofan engines has identified numerous
noise-generating mechanisms associated with the rotor blades and stator vanes. Tyler
and Sofrin (ref. 1) presented results which indicated that aerodynamic wakes leaving
the rotor may interact with stator vanes to set up complex pressure patterns in the
inlet duct. Hanson (ref. 2), by using random-pulse-amplitude and position-modulation
theory, studied the far-field noise resulting from the interaction of the rotor vis-
cous wakes with stator vanes in subsonic axial-flow fans. Researchers generally
recognized that static testing of turbofan engines usually produced far-field noise
levels which were greater than those obtained from flight. Many studies (refs. 3
to 8) suggested that inflow turbulence and shroud boundary-layer effects were some of
the causes of these high noise levels. These studies resulted in the development of
inflow-turbulence control devices and produced significant insight into simulating
flight noise with static tests.

Concurrent with this noise research, which tended to concentrate on far-field
noise and its relationship to the source noise, researchers were studying the source
mechanisms within the turbofan as they related to the rotor-wake defect structure,
rotor-tip vortex shedding, support-strut potential field, and separation distance
between the rotor and the stator vanes downstream of the rotor. References 9 to 15
are a few of the research efforts studying various aspects of these mechanisms. Both
analytical and experimental studies using various types of wake-survey, rotor and
stator-response instrumentation have been conducted. Fan rigs which produced experi-
mental data were designed or chosen for research so that hardware complications would
be kept to a minimum, thus permitting researchers minimal compromise with analytical
work. The analytical work has generally been based on incompressible flow with two-
dimensional compact source strip theory as applied to the rotor blades and stator

vanes. References 16 and 17 have extended the analytical work to include some compressible-flow effects with noncompact source distribution.

Most experimental research has been done on a basic fan rig, although references 5, 9, and 14 have indicated a need for experimental data on a "real engine." Additionally, within the large body of fluctuating pressure data taken from stator-vane studies, very few reliable data have been reported in a spanwise direction. The methodology has usually been to measure fluctuating pressures along the chord line at midspan of a stator vane and to assume knowledge of the spanwise distribution.

The National Aeronautics and Space Administration (NASA) has recognized the need to study the simulation effectiveness between the noise generated by a turbofan engine when mounted on a static test stand and that generated in flight. To address this need, NASA initiated an experimental research program using a highly instrumented JT15D-1 engine[1] which had been been slightly modified. Numerous results of the program have been reported. These results have been relative to the inflow-control-device comparisons (refs. 6 and 7); to the development of a measurement technique to convert nonstationary flight noise into narrow-band stationary noise (ref. 18); and to the effects of static, simulated forward speed and flight tests on both unsteady fan-blade pressures and acoustic far-field radiation (refs. 19 to 22).

An objective of the program was to study the rotor-induced fluctuating pressure levels (FPL) and their distribution along the span of both the core- and bypass-stator outlet guide vanes of this engine. The purpose of this report is to present the results of meeting this objective, thus fulfilling the need for spanwise data which has often been expressed. (See refs. 5 and 14.) The present data, obtained under static and flight conditions, are unique and provide the opportunity to study experimentally the stator-vane response under two widely different test conditions for an actual engine. The data are analyzed by using time histories, the signal-enhancement technique, narrow-band spectra, probability-density-function analysis, and phase- and coherence-function analysis. Comparisons between the static and flight results are made.

SYMBOLS AND ABBREVIATIONS

A   maximum altitude

BPF   blade-passage frequency

BW   bandwidth, Hz

F_1 fundamental tone associated with BPF of low-speed fan

$2F_1$ first harmonic of F_1

F_2 fundamental tone associated with BPF of high-speed compressor

$2F_2$ first harmonic of F_2

F_1 BPF   low-speed fan-rotor blade-passage-frequency fundamental tones

---

[1]Manufactured by Pratt & Whitney Aircraft of Canada.

2

F_2 BPF	high-speed-compressor blade-passage-frequency fundamental tones
FPL	fluctuating pressure level, $(2.9 \times 10^{-9}$ psi$)$, dB
f	frequency, Hz
n(t)	random noise, Gaussian distributed
PDF	probability density function
PDR	probability density ratio
p(x)	probability density
R	ratio of sine variance to noise variance, σ_s^2 / σ_n^2
RTV	rubberized coating
SMT	stator-mounted transducer
s(t)	sine signal, $A \sin(\omega t + \phi)$
T_a	time period of data analysis, sec
t	time, sec
x	amplitude
$\gamma^2(f)$	coherence function
ΔFPL	static-minus-flight fluctuating pressure level, dB
ΔPDR	static-minus-flight probability density ratio
δ	solidity
σ_n	standard deviation of noise signal, mV
σ_n^2	variance of Gaussian-distributed random noise, mV^2
σ_s^2	variance of sine signal, mV^2
ϕ	random phase angle, deg
ω	radian frequency, $2\pi f$

DESCRIPTION OF EXPERIMENT

Engine

The test engine, shown in the photograph and sketch of figure 1, was a JT15D-1 two-spool turbofan engine. It basically was an early-production model with the

design features summarized in table I. The engine had been modified (see table I) so that the rotor-interaction tone with the core-stator vanes would be acoustically cut off and produce lower broadband noise.

Figure 1(b) shows some features of the test engine. The inlet used in the static tests, although not the one used in flight, was made of fiberglass to the dimensions of the flight inlet. Six support struts, which are located in front of the centrifugal core compressor, are positioned behind the core/bypass-stator assembly. The sketch also shows a muffler fitted to the aft portion of the engine. The muffler used during the static tests had a different design from that used in flight. The purpose of using a muffler in these tests was to reduce or eliminate any aft noise radiation from the bypass duct which might compromise measurements of the front-end radiated fan noise.

Two photographs of the rotor blades are presented in figure 2. Typical metal angles and dimensions, as measured on this engine, are presented in table II. A characteristic affecting the flow through the blades is the raised portions on the pressure and suction sides of the rotor. The largest raised surface (sometimes referred to as a clapper) is designed to be in close proximity with a counterpart surface on the opposite side of an opposite blade. (See fig. 2(a).) Once the engine is spinning at about 2000 rpm, the rotor blades assume a position on the hub so that these raised surfaces touch each other, thus stiffening the rotor blades. The other raised portion had a different design from that of the clapper which additionally stiffened the blade. Figure 2(b) shows that the blades have a high degree of twist and a considerable variation in both the metal inlet and outlet angles. This figure also shows the core-stator vanes and the wall separating the core duct from the bypass duct. This wall is located just downstream of the rotor blades.

Figure 3 presents both a photograph of the stator assembly showing the core and bypass vanes and a sketch identifying the measurement transducers and their locations. The photograph (fig. 3(a)) shows the split bypass vanes along with the transducer positions. Table II also presents metal angles and associated stator dimensions as measured on the engine.

Test Facilities and Setup

Static test.- A photograph of the engine mounted on the outdoor test stand at the Ames Research Center is shown in figure 4. The engine was mounted so that it was 15 ft above the concrete surface of the test area. For the results presented in this report, no inflow control device covered the inlet. Far-field noise-measurement microphones situated on poles and on a traverse rail may be seen. These microphones were placed approximately 12 ft from the engine fan face. (See ref. 20.)

Flight test.- Figure 5 shows the research engine suspended beneath the wing of the test aircraft. The aircraft (a twin-engine OV-1B) was flown with the starboard T53 turboprop engine shut down and feathered to minimize inflow distortion during data acquisition for the operation of the JT15D-1. Results of the far-field noise measurements may be found in reference 21.

Test conditions.- Tests were conducted at the outdoor test site during a time period when surface wind speeds were less than 6 knots and the ambient temperature was approximately 62°F. Data were obtained at four nominal engine speeds of 6750, 10 500, 12 000, and 13 500 rpm.

During the flight tests, the test-bed aircraft was flown at a constant altitude of 300 ft with the flight speed maintained at a constant nominal 130 knots. Wind speeds from the surface to the flight altitude were less than 10 knots, and temperatures measured from the surface up to the flight altitude were a nominal 60°F. For these flight tests, engine speeds ranged from a nominal 6700 rpm to approximately 15 000 rpm.

Instrumentation

Description and mounting of pressure transducers.- Figure 3 presents a photograph and sketch identifying the locations of the miniature pressure transducers used in these tests. These transducers had a 0.04-in-diameter sensing area with a sensitivity of 1 V/psi. For this application there is an estimated accuracy of ±3 dB because of the harsh environment. The stator-mounted transducers (SMT), with individual locations denoted by letter designations A to E, were bonded to the surface of the pressure side of the vanes along the span and 0.15 in. from the vane leading edge. Two transducers were mounted at locations A and E (fig. 3(b)) so that they would be in the boundary layer of either the rotor hub or the bypass-duct outer wall. The SMT's were bonded with a rubberized material (RTV). Figure 6(a) presents a sketch of the mounting technique which shows the bonding material covering the transducers. This technique was used to protect the transducers from any foreign objects which may be contained in the airflow. The total thickness of the projection above the vane surface was no greater than 0.014 in. This mounting technique was evaluated and determined to present minimal interference with the measured pressures. (See ref. 23.)

Data-acquisition system.- Figure 6(b) shows a sketch of the data-acquisition instrumentation. Signals from the stator transducer were transmitted through a hard-wired system in the engine to signal-conditioning and analog frequency-modulated magnetic tape-recording equipment. The sketch also shows that a signal was recorded which gave the position of an instrumented rotor blade. This once-per-revolution pulse permitted the accurate measurement of fan speed and the application of the signal-enhancement technique to study the fluctuating-pressure data. The complete measurement system of figure 6(b) had a flat response over the frequency range from 20 Hz to 20 kHz. The dynamic range of the system was 120 to 170 dB.

During the flight tests, aircraft variables (speed, altitude, roll, etc.) and JT15D-1 engine variables (fuel flow, inlet and bypass pressures and temperatures, etc.) were measured and recorded by using a digital-pulse code-modulated system. Details on all signal-conditioning and data-acquisition systems onboard the aircraft may be found in reference 24.

RESULTS AND DISCUSSION

All data were processed over a frequency range from 0 to 20 kHz by using a fast Fourier transform, dual-channel analyzer and peripheral equipment to obtain averaged pressure time histories, narrow-band constant-bandwidth spectra, signal enhancement, probability functions, coherence, and phase information. All spectral data have an analysis bandwidth of $BW = 50$ Hz and were analyzed for more than 3 sec. This procedure insured that the random error was always less than ±1.5 dB with a 90-percent confidence level. The relationships of these data as a function of engine speed, and with respect to their spanwise locations, were studied and are discussed in this section.

Static-Test Results

The initial study of the pressure data took the form of considering the amplitude of pressure as it varied with time. Two techniques for studying these data are as follows: (1) determining the unenhanced average pressure per increment of time, and (2) determining the signal-enhanced pressure per increment of time. Although the former is accomplished by averaging a defined number of samples of pressure over a time period which is not synchronized with the rotor revolution, the signal-enhancement technique uses a once-per-revolution pulse to permit the synchronous averaging of the pressure as it varies with time relative to the engine rotational speed. This results in averaging out any contaminating noise and presents the periodic portion of the averaged pressure time trace. (See ref. 25.) Since the measured pressures are essentially the results of periodic wakes shed from the rotor blades, it was expected that the unenhanced pressure time trace (method 1) would appear to be strongly sinusoidal at the fan-rotor blade-passage frequency, hereinafter referred to as BPF and designated as F_1.

Figures 7 and 8 show some typical measured unenhanced and enhanced results of pressure time traces displayed in a 4-msec time increment. Figure 7(a) shows some unenhanced average pressure time traces measured at location D at engine speeds of 12 000 and 13 500 rpm for the static tests. At 12 000 rpm, the data suggest that a strong tone is present; however, the presence of a tone at 13 500 rpm is not so well-defined. Figure 7(b) shows the results of signal enhancing the data measured at location D for the four engine speeds of the static test. By comparing the unenhanced data in figure 7(a) at 12 000 rpm with its enhanced counterpart in figure 7(b), it may be seen that a sinusoidal signal tends to compose the signal in figure 7(a). The data comparison of figure 7 at 13 500 rpm does not make such a clear distinction. Additionally, by comparing the data in figure 7(b) for the four different engine speeds, one may see that not only does the amplitude vary but also the wave-shape changes of the pressure trace do not appear as smoothly increasing frequency patterns as the engine speed increases.

Figure 8 indicates the changing character of the stator response in a spanwise direction. This figure compares the signal-enhanced data of pressure time traces for a constant engine speed of 13 500 rpm for both the core (A,B) and bypass (D,E) locations. The figure indicates that a spanwise difference in wave shape is measured at each location on the core and bypass stators. Thus, the stator fluctuating-pressure data of figures 7 and 8 show pressure-trace differences at a singular stator location as a function of engine speed and differences in shape along a radial spanwise direction at a constant engine speed. These data, believed to be unique, are similar in appearance and may be related to aerodynamic results, whereby hot-wire anemometry techniques were used to measure the velocity-defect flow profiles behind rotors and ahead of stators. (See refs. 9 to 14 and 26.)

In order to measure the magnitudes of the unenhanced fluctuating pressures at the fan-rotor BPF and at its harmonics on the stator vanes, narrow-band spectral analyses (BW = 50 Hz) were obtained for the static and flight tests. Figures 9 and 10 present the results for the static tests. Figure 9 shows the spectra for the core (A,B), and figure 10 shows the spectra for the bypass (D,E) for the range of engine rotational speed. Data for location C are not available for presentation. These spectra indicate the presence of the fan-rotor BPF, related harmonics (or lack of them), and combination tones (indicated by F_1, $2F_1$, etc.). Large multiple frequencies below 3 kHz at radial locations D and E for 13 500 rpm are believed to be the result of aerodynamic shocks created by the supersonic rotor-blade tip speed. (See ref. 21.) Also, the data show responses at blade-passage frequencies compatible

with those of the high-speed compressor (designated as F_2). Although the aerodynamic wakes shed from the fan rotor impact on the stators and generate the F_1 frequencies, this would not be the case for the high-speed compressor. (See fig. 1(b).) The F_2 BPF tones are generated by the core-compressor fan blades cutting the wakes shed from the engine support struts ahead of the compressor. (See ref. 6.) Acoustic pressures at these F_2 BPF tones have been measured in the far field. (See refs. 6 and 19.) Because of this, the fluctuating pressures at the F_2 BPF seen in figures 9 and 10 are thought to be acoustic. The magnitudes of the F_2 FPL's are generally larger for the core locations than for the bypass locations, which would be reasonable for this test configuration.

Figure 11 compares the core and bypass FPL's at the F_1 BPF obtained from figures 9 and 10. The data show a signal which is generally above the broadband noise by approximately 10 dB or more with the levels for both stators falling between 140 and 165 dB. The broadband noise levels were plotted to permit a later comparison with flight. These levels, which were measured at the base of the tones, are often said to be associated with the turbulence of the rotor wakes. (See ref. 25.) Figure 11 also shows an obvious difference between the core data and the bypass data. As the engine speed increases, the core data tend to increase in amplitude, whereas the bypass data have a dip at 10 500 rpm.

To investigate the change in fluctuating pressures at the rotor BPF across the core- and bypass-stator span, the FPL's were plotted as a percent of span length and are presented in figure 12. Figure 12(a) shows that for locations A and B on the core-stator vanes, changes on the order of 5 to 10 dB occur, either rising or dropping as a function of engine speed. An exception occurs at 10 500 rpm where the spanwise distribution is flat. For the bypass stator (fig. 12(b)), it can be seen that when moving radially outward from location D to E, increasing fluctuating pressures are measured. It is also observed that the lowest and the least change in pressure magnitudes occurs at 10 500 rpm.

Figure 13 presents the F_2 FPL measured on the core and bypass stators for the engine speeds of the static tests. As mentioned previously, the signal is believed to be acoustically related to the core compressor. It is observed that the core data seem to have a better ratio of signal to noise than the bypass data, neither of which is as good as the ratios in figure 11. It can be seen that the F_2 FPL data seem to be more consistent in increasing in level as engine speed increases than the F_1 FPL data. It may also be observed that the magnitudes of the F_2 FPL data in the core are larger than in the bypass, with no measurable tone at location E at a speed greater than 6750 rpm.

Hanson (ref. 2) has discussed the turbulence associated with the aerodynamic velocity defect of the wake shed behind a rotor blade. This wake may have both an amplitude and a position modulation. The position modulation is usually small; however, the amplitude modulation may be several orders of magnitude greater than the average magnitude. Thus, in lieu of a pure sinusoidal-wave character seen by the stator at the rotor BPF, a signal such as that presented in figure 7(a) may be observed. Signal enhancement (such as that presented in figs. 7(b) and 8) may do little to improve the wave shape. Data such as that in figures 7 or 8 could be either narrow-band random noise or random noise which contains a pure tone. A narrow-band spectral analysis of data, such as that in figures 7 or 8 (as presented in fig. 9 for unenhanced pressures), would not by itself determine if a tone contained in noise was of steady or unsteady amplitude. As part of the analysis of the data obtained for this report, it was desirable to investigate the amplitude

stability of the fan-rotor BPF tones (such as those seen in the spectra of fig. 9) for the static and flight cases.

References 10 and 25 discussed the use of performing a narrow-band analysis of the enhanced pressure time signal and comparing the magnitude of the BPF from the resulting spectrum with that obtained from the spectrum of the unenhanced pressure time signal. For constant engine speeds, this permits an estimation of the amount of unsteadiness or randomness in the fluctuating pressure level at the BPF in the periodic portion of the pressure time signal. It was noted in reference 20, however, that it is very difficult to maintain a constant fan speed when testing outdoors without an inflow control device. When the engine speed changes, phase changes in the signal measured by the stator transducers may be expected to occur. Since the static-test data in the present report were obtained without an inflow control device, the application of the signal-enhancement technique available during this analysis would not account for phase changes resulting from fan-speed changes. Additionally, the comparison of the spectral analysis of signal-enhanced and signal-unenhanced pressures cannot account for the random phase variations which may occur in the signal. (See ref. 27.) References 5 and 28 discuss this ensemble-averaging technique and compare it with the application of the probability-density-function (PDF) analysis technique. The PDF analysis permits one to determine if there is a tonal signal added with noise as well as a measure of how unsteady or random the amplitude is. Since the PDF considers only the signal amplitude, it is not susceptible to any fluctuation in frequency or engine rotational speed (such as the ensemble-averaging technique) or to any random-phase variation which may occur.

The PDF analysis is based on the fact that a dish-shaped probability density function will result for a constant-amplitude sinusoidal wave and that a Gaussian-shaped probability density function will result if the wave is narrow-band random noise. Thus, if the two signals are combined so that a stationary and ergodic random-noise time history appears in the form of

$$x(t) = n(t) + s(t)$$

where $n(t)$ denotes a Gaussian random noise and $s(t)$, a sine signal with random phase angle ϕ and maximum amplitude A, is given by

$$s(t) = A \sin(\omega t + \phi)$$

it has been shown (ref. 27) that the probability density of $x(t)$ is

$$p(x) = \frac{1}{\sigma_n \pi \sqrt{2\pi}} \int_0^\pi \exp\left[-\left(\frac{x - A \cos \phi}{4\sigma_n}\right)^2\right] d\phi$$

If the variance of the sine signal is σ_s^2 and that of the noise is σ_n^2, the ratio of the two will be

$$R = \sigma_s^2 \Big/ \sigma_n^2$$

Typical plots of $p(x)$ for different values of R are presented in figure 14. This plot shows that as R increases, the signal becomes increasingly sinusoidal with a constant amplitude. The ratio R may be plotted as a function of the probability density ratio PDR as determined by measuring the ratio of the average magnitude of the side peaks to the magnitude of the minimum density at $x = 0$ as shown in figure 15. This figure shows that as the PDR increases, the amplitude of the tone becomes increasingly stable. Thus, by measuring the PDR, a good qualitative estimation of the stability of the tone may be assessed. In contrast to the limitation of the signal-enhancement technique discussed earlier, the limitation of the PDF analysis is the insensitivity to a PDR of unity. With these considerations in mind, the PDF analysis was used to study qualitatively the degree of amplitude steadiness in the tones. To ensure that the analysis error was well below that of the measurement error of the transducers, the PDF of the F_1 and F_2 BPF's was obtained by measuring the resulting signal after the overall signal had been bandpass filtered with a 7-percent bandwidth of the BPF. The analysis time T_a was always such that the minimum criterion of $T_a > 50/BW$ was exceeded by a factor of 10. Thus, the analysis error was estimated to be approximately less than or equal to 1 percent of the true PDF.

Figure 16 presents examples of a typical set of PDF data for the static test at 12 000 and 13 500 rpm for the pressures measured on the core stator at location A. It can be seen that the PDF of the signal at 13 500 rpm appears to be almost Gaussian shaped with an estimated PDR equal to 1.1. At 12 000 rpm, the PDF shows that a strong, constant amplitude tone is contained in the signal with the PDR equal to 1.5.

Figure 17 presents a graphic display of the PDR as a function of the engine rotational speed for the static tests. The PDR data are presented for the core-stator locations in figure 17(a) and for the bypass-stator locations in figure 17(b). A comparison of the two data sets indicates that the core F_1 tones tend to be less stable, with less fluctuation in stability as speed increases, than the bypass tones. Thus, the core F_1 tones are obscured by random noise, are themselves narrow-band random noise, or have unsteady amplitudes. Generally, the bypass F_1 tones do not seem to be narrow-band random noise but do appear to fluctuate in strength of amplitude stability.

Although not presented, the PDF analysis of the high-speed-compressor F_2 BPF tone data showed all amplitudes to be Gaussian distributed. This would be compatible with acoustic signals which would propagate through a turbulent-flow environment, such as that which exists from the core compressor to the bypass-stator area.

Flight-Test Results

For the flight tests, stator-pressure data were obtained for 10 different engine speeds from a nominal 6700 rpm to approximately 15 000 rpm. The narrow-band (50-Hz BW) spectra of the unenhanced pressures measured at each location on the stators for each engine speed are presented in figure 18. The data show the BPF for the low-speed fan (F_1) and high-speed compressor (F_2) with the related harmonics and combinations of F_1 and F_2.

The data are presented in figures 19 to 21 to indicate how the magnitudes of the FPL's changed for the F_1 BPF as a function of engine speed and spanwise location. Figure 19 compares the core and bypass levels as a function of engine speed. This figure shows the core pressures at the fan-rotor BPF (F_1) for locations A and B to be

quite different from the bypass pressures measured at locations C, D, and E. The core FPL's remain about 10 dB above the broadband levels and smoothly increase as the engine speed increases. The broadband FPL's for the bypass data have about the same magnitude and trend with engine speed as those for the core. The FPL's at the F_1 BPF for the bypass locations, however, show a large fluctuation of values for increasing engine speed. Rapid changes in level for all bypass locations occur as the engine speed moves from 9525 to 10 917 rpm. Behavior in this region is thought to be inconsistent with behavior which may be due to wake changes alone. Thus, nonuniformities in rotor exit flow and aeroacoustic phenomena may be influencing the stator pressures. (See refs. 25 and 29.)

Figures 20 and 21 present the spanwise distribution of the F_1 fluctuating pressure levels at the BPF for the engine speeds obtained during the flights. Figure 20 shows that along the core span, there is a uniform fluctuating pressure at the BPF. There is a slight decrease in magnitude in a radial direction at any one engine speed except at 13 296 rpm, where there is a rapid rise in level. This general uniformity is not apparent for the spanwise distribution of the bypass data presented in figure 21. This figure shows that at the three highest speeds of 14 880, 13 296, and 11 919 rpm, there tends to be a uniform fluctuating pressure on the stators except at the tip location E, where a 10-dB rise occurs at 11 919 rpm. There is a constant decrease in the fluctuating pressure for the engine rotational speeds between 10 917 and 9525 rpm as the position radially changes from location C to E. The lowest speeds of 8927, 8324, and 6708 rpm tend to exhibit a spanwise increase in the FPL's, which is initially rapid for 8927 and 8324 rpm.

The steadiness of the amplitudes of these F_1 BPF's were investigated in an attempt to gain an insight into the fluctuating-pressure data. Figure 22 shows the PDR of the core and bypass data as a function of the engine speed. The core data (fig. 22(a)) show that as the engine speed increased, the steadiness of the F_1 amplitudes generally increased, thus indicating less turbulence or an increase in amplitude stability. This is not seen in figure 22(b) which shows that as the engine speed increases, the unsteadiness of the amplitudes of the BPF's increase; that is, there is a general decrease in PDR, thus indicating greater turbulence or a decrease in amplitude stability.

The FPL's associated with the high-speed-compressor blade-passage frequency (F_2) were measured for the flight case and are presented in figure 23 as a function of the engine speed. These data, as discussed earlier, are believed to be acoustic pressures and can be seen to have a greater magnitude in the core area (fig. 23(a)) than in the bypass area (fig. 23(b)). Additionally, all PDF's of the F_2 data were analyzed and observed to be Gaussian shaped, a characteristic of narrow-band random noise.

It is believed that the core FPL's exhibit different characteristics from the bypass FPL's because of differences between the flow distributions which exist around the spinning-rotor hub, within the core duct, and within and along the walls of the bypass duct. These flow differences would result from hub and wall boundary-layer effects, flow separation and vortex shedding from rotor blades, rotor-blade tips cutting through the bypass-duct wall boundary layer, and secondary flow. (See refs. 9 to 16.) Additionally, it is known that a radially asymmetrical wake profile is likely to exist behind a rotor blade (refs. 12, 26, and 30) and that the blade stiffeners affect the flow and pressure losses over the fan blade (ref. 31). The common wall shared by the core and bypass ducts, although unknown in its effects, is expected to complicate further the interpretation of the measured pressures. Finally, this nonuniformity of the spanwise distribution of the core and bypass FPL's

may be related to wake variance from rotor blade to rotor blade, which is caused by blade-geometry variance due to fabrication and uneven wear.

For the flight data, cross-spectra techniques were used to obtain coherence and phase information about the signals. In particular, it was desirable to compute the trace velocity of possible acoustic or convected wake speeds along the stator spans. If this could be accomplished, it was anticipated that secondary or three-dimensional flow, as well as acoustic pressure signals, could be firmly established.

Typical results of the coherence and phase measurements are presented in figures 24 to 26 for the three engine speeds of 13 296, 11 919, and 10 434 rpm. These speeds were chosen to represent supersonic, transonic, and subsonic blade tip speeds, respectively. For some of the data in these figures, coherence blanking was used at the 0.5 level. Thus, when used, only coherence values greater than or equal to 0.5 were displayed. It can also be noticed that the phase data show an expanded scale when compared with the coherence-frequency scale. This was done to try to display the phase measurements more clearly. The data of figures 24 to 26 are presented to indicate the complex environment of the stators. The coherence data may be seen to be generally low (below 0.5) for most frequencies except for the F_1 BPF, some F_1 harmonics, and some of the F_2 BPF harmonics. For the low-coherence values, there is a significant degree of nonrelatedness between the two signals and there is a larger random error than if the signals are highly coherent ($\gamma^2(f) > 0.7$). Additionally, the phase data associated with the coherence data generally show significant scatter at frequencies above the F_1 BPF. Interpretations of these data are limited because of two reasons: (1) Low-coherence values have large random errors associated with the measured phase, and (2) high-coherence values for the F_1 BPF and its harmonics have no consistent phase relationships.

Regardless of these difficulties, several interesting observations may be made about the results. Figure 24 presents the coherence and phase relationships for the pressures measured at the core-stator locations. This figure shows that a high coherence (above 0.7) existed between locations A and B at both the F_1 BPF and $2F_2$ BPF for the three engine speeds. This implies that at these frequencies the pressures are linearly related. At several other frequencies which do not seem to be related to the F_1 or F_2 compressor, the coherence may be seen to be high, showing a high degree of relatedness of the pressures at these frequencies. The significance of this, however, is unclear.

The data reduction was designed so that a positive slope for the phase data would indicate flow moving radially outward and a negative slope would indicate flow moving radially inward. The phase relationships between the pressures measured at locations A and B in figure 24 show wide scatter at the frequencies above the F_1 BPF and little significance at the other frequencies where there is low coherence. Thus, although the slope of the phase response up to the F_1 BPF of the core data may appear positive, caution is suggested in interpreting this as radially outward flow.

The coherence and phase pattern for the pressures measured on the bypass stator at locations C and D (fig. 25) show the same type of information. Coherence is low (below 0.5) at most frequencies except for the F_1 BPF and some of the harmonics. At the subsonic speed, the third harmonic of the high-speed compressor ($3F_2$) is seen to have a high coherence. Thus, it appears that there is a linear relationship only at the BPF, at some of the harmonics of the low-speed compressor, and at the third harmonic of the high-speed compressor. The phase data show a generally negative slope up to about 4000 Hz and then exhibit large scatter. This suggests a cautious interpretation of possible turbulent flow moving radially inward.

11

Data showing the coherence and phase relationship between the pressures measured at the D and E locations are presented in figure 26. Especially high coherence (larger than 0.8) is seen at the subsonic and supersonic speeds for the low-speed-fan BPF (F_1) and its harmonics and for the high-speed-compressor BPF ($2F_2$) at the second harmonic. At the transonic speed, the F_1 BPF coherence is not very high (0.65).

Thus, the data of figures 25 and 26 suggest a strong linear relationship between the pressures measured by the bypass transducers at subsonic and supersonic blade tip speeds but a considerably reduced linear relationship at transonic blade tip speeds for the F_1 BPF pressure. The phase data suggest a flat-slope inphase relationship below about 4 kHz for the subsonic blade tip speed, where the coherence appears to be larger than 0.7. This is not believed to be representative of secondary flow. The data above about 4 kHz for the subsonic speed, and for all frequencies at the transonic and supersonic blade tip speeds, either exhibit large scatter or may not be reliably interpreted because of the low-coherence values.

Although the flight data of figures 24 to 26 show high-coherence values at the rotor BPF and its harmonics, the wide scatter of the phase data and low-coherence values precluded any meaningful interpretation of wave-trace velocities. Similar behavior has been reported for some static tests. (See ref. 5.) Such behavior is attributed to the severity of the environment, that is, turbulent flow and hard reflecting surfaces. (See refs. 5 and 25.)

Comparison of Static and Flight Results

Some comparisons of the static data with the flight data for the fan-rotor F_1 BPF tone (figs. 11 and 19) for comparable engine speeds are presented in figures 27 and 28. Figure 27 shows that the core-stator static, and flight data appear to have the same trend. Thus, both the static and flight FPL's at the F_1 BPF for core locations A and B appear to increase generally up to approximately 12 000 rpm, where the pressures at location A then appear to drop in value at the next higher engine speed. The pressures measured at location B, however, tend to increase dramatically for the next higher engine speed. As discussed earlier, these core data of figure 27 do not have the same trend as the bypass data. A comparison of the bypass-stator static and flight data are presented in figure 28 as a function of engine speed. This figure shows the narrow-band FPL's at the fan-rotor F_1 BPF tone as measured at locations D and E. The data for location E show the same general trend for the static and flight tests; however, trend differences between the static and flight data for location D are evident for increasing engine speeds.

One may compare the spanwise distributions of the narrow-band FPL's of the F_1 BPF tones for the static and flight data by replotting some of the data presented in figures 12, 20, and 21. These static and flight comparisons are presented in figures 29 and 30 for data that were measured at comparable engine speeds and locations. Figure 29 shows that for the core data, the static tests showed increasing levels in a radially outward direction for engine speeds of 6750 and 13 500 rpm, decreasing levels at 12 000 rpm, and constant levels at 10 500 rpm. The flight data show only one engine speed, 13 296 rpm, which results in an increasing FPL in a radial direction. The FPL's decrease radially outward for 11 919 and 10 434 rpm and appear constant for 6708 rpm.

Figure 30 presents a similar spanwise-distribution comparison of the static and flight data for the bypass stator. The static-test data show, for locations D and E, increasing levels in a radially outward direction for engine speeds of 6750, 10 500,

12 000, and 13 500 rpm. At the comparable flight-test speeds, the flight data exhibit slight, radially outward increases in FPL at 6708 and 13 296 rpm, a sharp decrease in FPL at 10 434 rpm, and a sharp, radially outward increase in FPL at 11 919 rpm.

The data of figures 27 to 30 suggest a complex environment in which the core and bypass stators are immersed. Thus, no clear trends seem evident for the variation of the FPL with engine speed or for the uniformity of the spanwise distribution of the FPL's on the core and bypass stators. As discussed earlier, this environment is believed to be the result of the differences in boundary-layer development along the rotor blades, differences in hub and bypass-duct wall boundary layers, suspected asymmetrical wake profiles due to the rotor-blade stiffeners, and three-dimensional flow.

Figures 31 and 32 present the differences in the magnitudes between the static and flight FPL's for the fan-rotor F_1 BPF tone and broadband noise. The flight levels were subtracted from the static levels and are presented as a function of engine speed. It is recognized that although the flight and static engine speeds are not equal, they are well within the experimental error associated with the amplitudes. Figure 31, which presents the static-to-flight differences for the F_1 BPF levels, shows that the largest portion of the differences lies above the zero reference line with the static tests producing higher amplitudes than the flight tests by about 5 dB. The same observation may be made about the associated broadband levels presented in figure 32. A possible reason for the higher static levels is that the operating line for the static tests was higher than for the flight tests, thus producing higher rotor loading. (See ref. 21.) Also, the engine did not have an inflow control device during the static tests. It is known that because of the nonisotropic nature of the inlet turbulence which occurs during the static tests, both tone and broadband acoustic noise levels are larger during static tests than during flight. (See ref. 3.) Additionally, reference 21 compared the tone and broadband far-field acoustic noise for this engine and showed the static data (obtained without an inflow control device) to be higher than the flight data.

The results of comparing the steadiness of the amplitudes of the fundamental tones as measured for the static and flight data (figs. 17 and 22) are presented in table III and figure 33. Table III shows that the strength of the tone is not as large for the core FPL's as for the bypass FPL's, and figure 33 shows that there appears to be some difference between the static and flight environment as measured by the stability of these tones. Thus, figure 33 appears to show that flight-tone amplitude stability is somewhat greater than static-tone amplitude stability.

CONCLUDING REMARKS

Stator-vane fluctuating pressures were measured on a highly instrumented, flight-certified JT15D-1 turbofan engine which was used in a program by the National Aeronautics and Space Administration to study forward-speed effects on fan-tone noise. These data, obtained for static and flight tests, are believed to be unique and help fill the need for information about stator-vane response for an engine in flight.

Pressure time traces (resulting from the aerodynamics of the rotor wakes) were measured at individual locations along the leading edge of both a core and bypass stator. Data were obtained which showed nonuniform changes in the amplitudes and wave shape of the pressure with respect to time for both a spanwise distribution of

13

these pressure traces at a constant engine speed and for these pressure traces at any one location for different engine speeds. The core spanwise distributions of the fluctuating pressure levels (FPL) at the fan-rotor blade-passage-frequency fundamental tones (F_1 BPF) were noticeably different from the bypass-stator FPL's as a function of engine speed. The nonuniformity of these data are believed due to the complex acoustic/aerodynamic flow environment.

The core-stator vanes exhibited fan F_1 BPF amplitudes with probability density ratios (PDR) lower than those for the bypass-stator-vane responses. This implies that they were not as stable as the bypass-stator-vane responses. A comparison of core and bypass PDR's with regard to static and flight conditions indicated that some difference existed, thus suggesting that the static environment may have produced more unstable amplitude tones than the flight environment. The magnitudes of the responses for the static tests were generally 5 dB greater than those for the flight tests. These results are believed to be due to the anisotropic nature of the inlet flow and higher rotor loading during the static tests. There was a high spanwise coherence between stator transducers for the fluctuating pressures at the fan BPF's which indicated that they were excited by the same forcing mechanism. Disturbance trace velocities however could not be interpreted at the BPF fluctuating pressures because of the complex environment.

Fluctuating pressures were detected on the stator vanes at blade-passage frequencies of the high-speed core compressor. These levels were higher on the core-stator vane than on the bypass-stator vane, and all fluctuating pressure levels had probability density functions typical of narrow-band random noise. These fluctuating pressures are believed to be acoustic since far-field acoustic tones at these high-speed-compressor fundamental tones (F_2 BPF) have been measured.

Langley Research Center
National Aeronautics and Space Administration
Hampton, VA 23665
February 16, 1984

14

REFERENCES

1. Tyler, J. M.; and Sofrin, T. G.: Axial Flow Compressor Noise Studies. SAE Trans., vol. 70, 1962, pp. 309-332.

2. Hanson, Donald B.: Unified Analysis of Fan Stator Noise. J. Acoust. Soc. America., vol. 54, no. 6, Dec. 1973, pp. 1571-1591.

3. Cumpsty, N. A.; and Lowrie, B. W.: The Cause of Tone Generation by Aero-Engine Fans at High Subsonic Speeds and the Effect of Forward Speed. Trans. ASME, Ser. A: J. Eng. Power, vol. 96, no. 3, July 1974, pp. 228-234.

4. Hanson, Donald B.: A Study of Subsonic Fan Noise Sources. AIAA Paper 75-468, Mar. 1975.

5. Bliss, D. B.; Chandiramani, K. L.; and Piersol, A. G.: Data Analysis and Noise Prediction for the QF-1B Experimental Fan Stage. NASA CR-135066, 1976.

6. McArdle, J. G.; Jones, W. L.; Heidelberg, L. J.; and Homyak, L.: Comparison of Several Inflow Control Devices for Flight Simulation of Fan Tone Noise Using a JT15D-1 Engine. NASA TM-81505, 1980.

7. Jones, W. L.; McArdle, J. G.; and Homyak, L.: Evaluation of Two Inflow Control Devices for Flight Simulation of Fan Noise Using a JT15D Engine. AIAA Paper 79-0654, Mar. 1979.

8. Atvars, Y.; and Rogers, D. F.: The Development of Inflow Control Devices for Improved Simulation of Flight Noise Levels During Static Testing of a HBPR Turbofan Engine. AIAA-80-1024, June 1980.

9. Gallus, H. E.; Grollius, H.; and Lambertz, J.: The Influence of Blade Number Ratio and Blade Row Spacing on Axial-Flow Compressor Stator Blade Dynamic Load and Stage Sound Pressure Level. Paper 81-GT-165, American Soc. Mech. Eng., Mar. 1981.

10. Fleeter, S.; Jay, R. L.; and Bennett, W. A.: Rotor Wake Generated Unsteady Aerodynamic Response of a Compressor Stator. Paper 78-GT-112, American Soc. Mech. Eng., Apr. 1978.

11. Magliozzi, B.; Hanson, D. B.; Metzger, F. B.; and Johnson, B. V.: Noise and Wake Structure Measurements in a Subsonic Tip Speed Fan. NASA CR-2323, 1973.

12. Shaw, Loretta M.; and Balombin, Joseph R.: Rotor Wake Characteristics Relevant to Rotor-Stator Interaction Noise Generation. NASA TM-82703, 1981.

13. Franke, G. F.; and Henderson, R. E.: Unsteady Stator Response to Upstream Rotor Wakes. AIAA Paper 79-0579, Mar. 1979.

14. Jay, Robert L.; and Bennett, William A.: The Effects of Solidity, Interblade Phase Angle and Reduced Frequency on the Time-Variant Aerodynamic Response of a Compressor Stator. AFOSR-TR-80-1041, U.S. Air Force, June 1980. (Available from DTIC as AD A090 546.)

15. O'Brien, Walter F., Jr.; Reimers, Stephen L.; and Richardson, Scott W.: Interaction of Fan Rotor Flow With Downstream Struts. AIAA-83-0682, Apr. 1983.

16. Kobayashi, Hiroshi; and Groeneweg, John F.: Effects of Inflow Distortion Profiles on Fan Tone Noise Calculated Using a 3-D Theory. AIAA Paper 79-0577, Mar. 1979.

17. Atassi, H.; and Hamad, G.: Sound Generated in a Cascade by Three-Dimensional Disturbances Convected in a Subsonic Flow. AIAA-81-2046, Oct. 1981.

18. Mueller, Arnold W.; and Preisser, John S.: Flight Test of a Pure-Tone Acoustic Source. NASA TP-1898, 1981.

19. Preisser, J. S.; Schoenster, J. A.; Golub, R. A.; and Horne, C.: Unsteady Fan Blade Pressure and Acoustic Radiation From a JT15D-1 Turbofan Engine at Simulated Forward Speed. AIAA-81-0096, Jan. 1981.

20. Schoenster, James A.: Fluctuating Pressures on Fan Blades of a Turbofan Engine – Static and Wind-Tunnel Investigations. NASA TP-1976, 1982.

21. Preisser, John S.; and Chestnutt, David: Flight Effects on Fan Noise With Static and Wind Tunnel Comparisons. AIAA-83-0678, Apr. 1983.

22. Schoenster, James A.: Fluctuating Pressure Measurements on the Fan Blades of a Turbofan Engine During Ground and Flight Tests. AIAA-83-0679, Apr. 1983.

23. Englund, David R.; Grant, Howard P.; and Lanati, George A.: Measuring Unsteady Pressure on Rotating Compressor Blades. NASA TM-79159, [1979].

24. Knight, Vernie H., Jr.: In-Flight Jet Engine Noise Measurement System. Paper presented at the ISA 27th International Instrumentation Symposium (Indianapolis, Indiana), Apr. 27-30, 1981.

25. Hanson, Donald B.: Study of Noise and Inflow Distortion Sources in the NASA QF-1B Fan Using Measured Blade and Vane Pressures. NASA CR-2899, 1977.

26. Atassi, H.: Effect of Loading and Rotor Wake Characteristics on the Acoustic Field of Stator Blades. AIAA Paper 76-566, July 1976.

27. Bendat, Julius S.; and Piersol, Allan G.: Engineering Applications of Correlation and Spectral Analysis. John Wiley & Sons, Inc., c.1980.

28. Piersol, A. G.; Wilby, E. G.; and Wilby, J. F.: Evaluation of Aero Commander Propeller Acoustic Data: Taxi Operations. NASA CR-159124, 1979.

29. Hanson, Donald B.: Study of Noise Sources in a Subsonic Fan Using Measured Blade Pressures and Acoustic Theory. NASA CR-2574, 1975.

30. Shreeve, R.; and Neuhoff, F.: Measurements of the Flow From a High Speed Compressor Rotor Using a Dual Probe Digital Sampling (DPDS) Technique. NPS67-82-010, U.S. Navy, Sept. 1982. (Available from DTIC as AD A122 432.)

31. Pickerell, D. J.: Rolls-Royce RB211-535 Power Plant. J. Aircr., vol. 20, no. 1, Jan. 1983, pp. 15-20.

TABLE I.- DESIGN FEATURES OF MODIFIED JT15D-1 ENGINE

Fan pressure ratio 1.5

Bypass ratio 3.3

Hub/tip ratio 0.405

Rotor diameter, in. 21

Maximum fan rotational speed, rpm 16 000

Rotor blades 28

Core-stator vanes 71

Bypass-stator vanes 66

Ratio of number of bypass-stator vanes to rotor blades 2.36

Ratio of number of core-stator vanes to rotor blades 2.54

Ratio of rotor-blade spacing to bypass-stator-vane spacing 1.83

Ratio of rotor-blade spacing to core-stator-vane spacing 0.63

Primary exhaust area, in^2 79

Bypass exhaust area, in^2 190

TABLE II.- METAL ANGLES AND DIMENSIONS OF ROTOR AND STATOR VANES
OF JT15D-1 ENGINE

(a) Rotor blade

Radial location above root, in.	Metal angles at blade locations, deg		
	Inlet	Stagger	Exit
0.30	44.0	17.0	-10.8
.55	45.5	21.4	4.0
1.25	49.8	33.7	12.7
2.50	51.4	45.2	27.8
3.75	58.5	52.6	43.7
3.99	59.7	54.2	45.2
4.74	63.6	58.3	49.8
5.00	64.9	61.0	51.4
5.24	66.3	62.6	53.2
6.20	73.2	69.1	60.4

(b) Stator vanes

Location	Metal angles at vane locations, deg		
	Inlet	Stagger	Exit
Core			
Root	-48.4	-31.3	-18.3
SMT A	-46.4	-31.2	-17.6
SMT B	-44.2	-30.6	-15.7
Tip	-40.4	-30.7	-13.3
Bypass			
Root	-39.0	-19.6	6.7
SMT C	-36.3	-16.9	7.1
SMT D	-35.5	-15.3	7.3
SMT E	-34.4	-14.0	7.4
Tip	-34.0	-14.5	7.5

(c) Dimensions

Component	Average chord, in.	Average span, in.	Solidity, δ
Rotor blade	2.4	6.2	
Core-stator vane	0.88	1.89	1.93
Bypass-stator vane ...	1.53	3.3	1.88

TABLE III.- COMPARISON OF MEASURED PROBABILITY DENSITY RATIO FOR STATOR
F_1 BPF FLUCTUATING PRESSURES AS A FUNCTION OF ENGINE SPEED

[Static and flight tests]

SMT	Probability density ratio at engine rotational speed of -							
	6750 rpm (static)	6708 rpm (flight)	10 500 rpm (static)	10 434 rpm (flight)	12 000 rpm (static)	11 919 rpm (flight)	13 500 rpm (static)	13 296 rpm (flight)
Core-stator vane								
A	1.0	1.2	1.2	1.3	1.5	1.5	1.0	1.0
B	1.0	1.0	1.0	1.0	1.0	1.2	2.1	2.4
Bypass-stator vane								
D	2.5	2.7	1.5	2.2	2.3	1.2	1.5	2.0
E	2.5	2.9	1.0	1.0	2.6	2.4	1.9	1.9
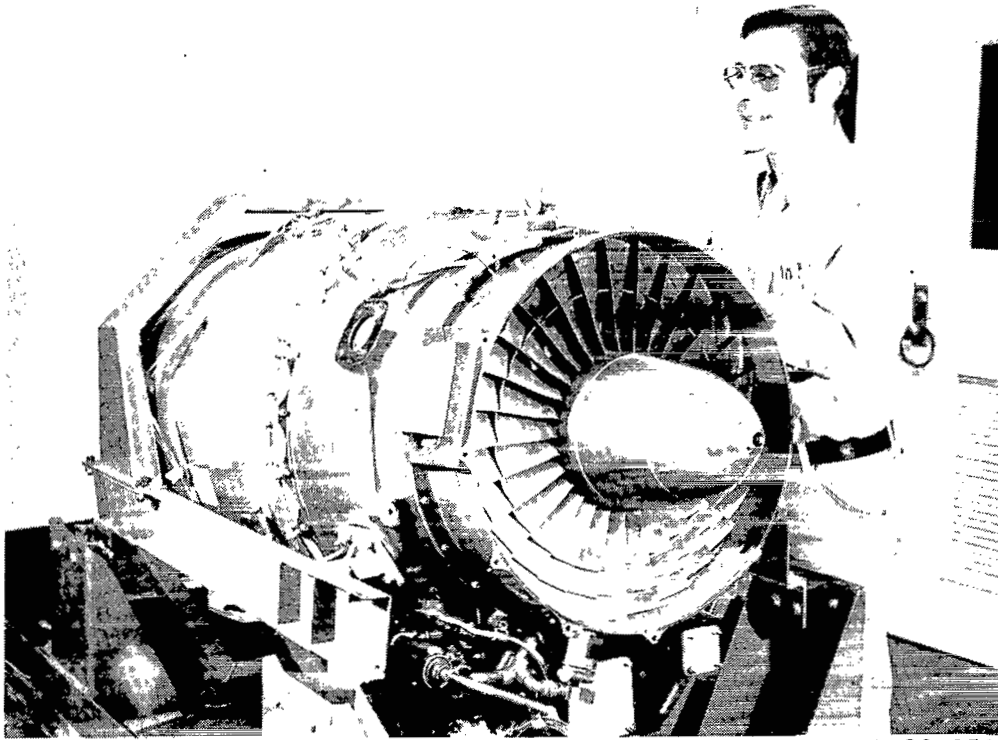
L-80-950

(a) Photograph of JT15D-1 engine with nacelle and inlet removed.
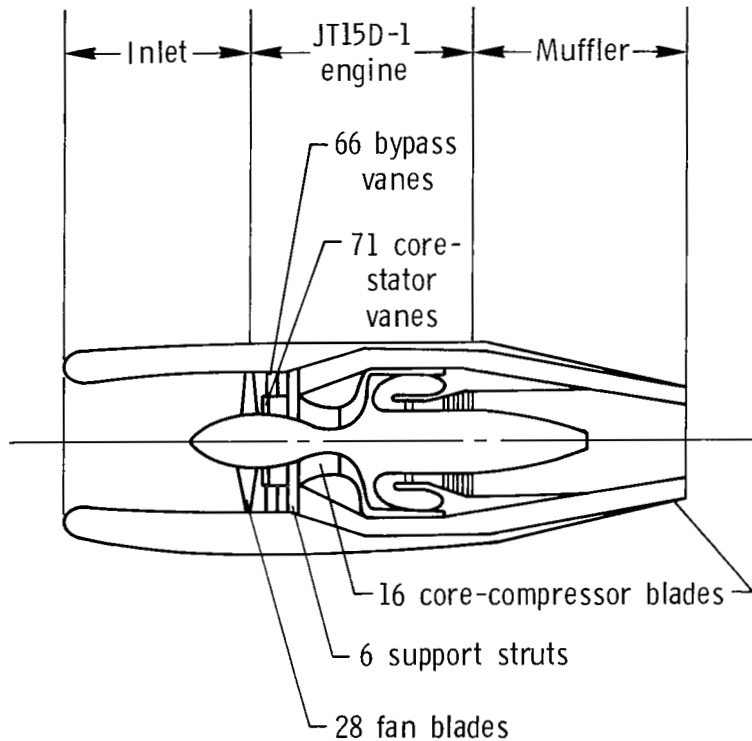
(b) Cross-sectional sketch of JT15D-1 engine in test configuration.

Figure 1.- Photograph and sketch of JT15D-1 engine used in static and flight tests.
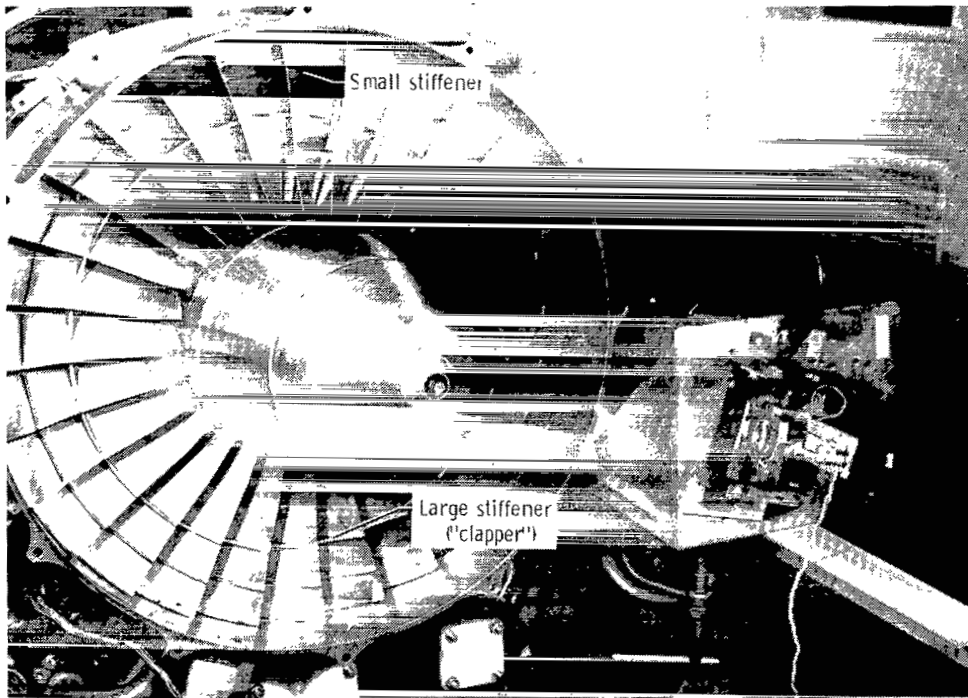
(a) Overall view of fan rotor blades.
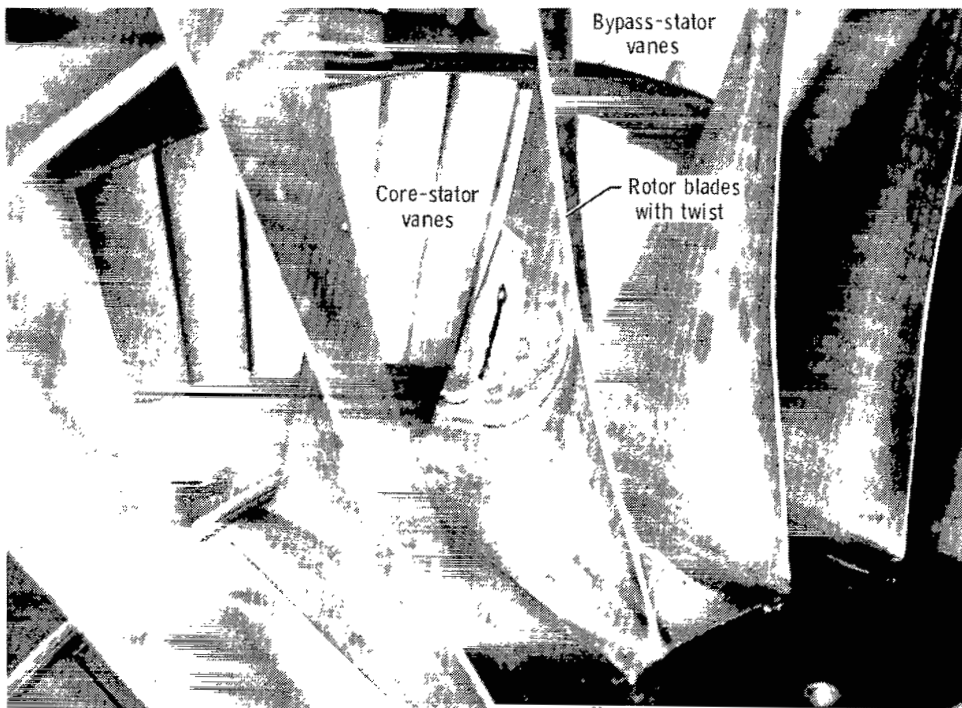
(b) Close-up view of fan rotor blades.

L-84-10

Figure 2.- JT15D-1 rotor-blade assembly.

L-80-896

(a) Stator-vane assembly.
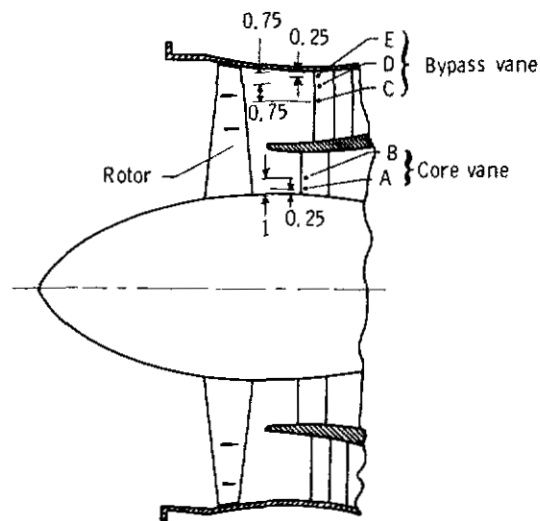
(b) Transducer locations. All transducers
are 0.15 in. from leading edge. All
dimensions are in inches.

Figure 3.- Photograph and sketch of stator-vane
assembly and transducer locations.
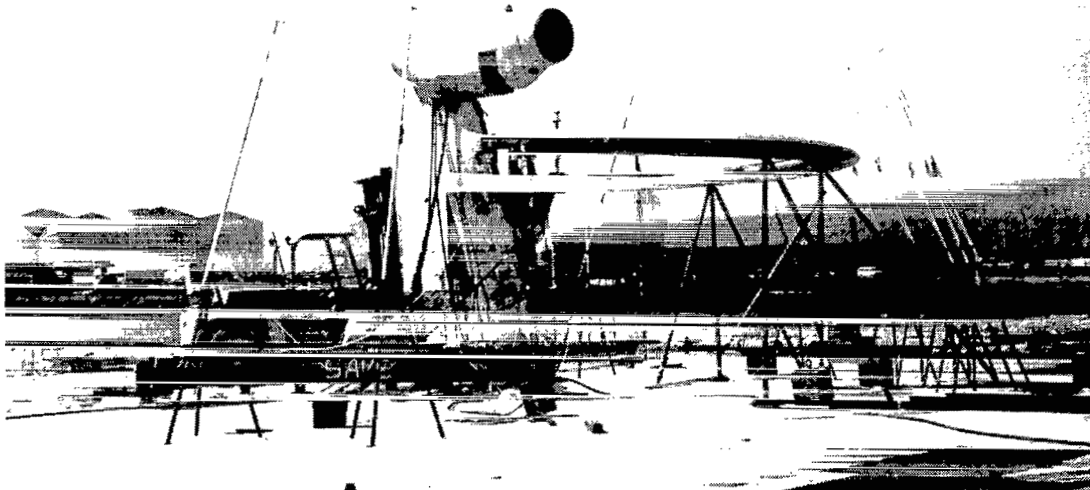
L-82-117

Figure 4.- JT15D-1 engine mounted on outdoor static-test stand at the
Ames Research Center.
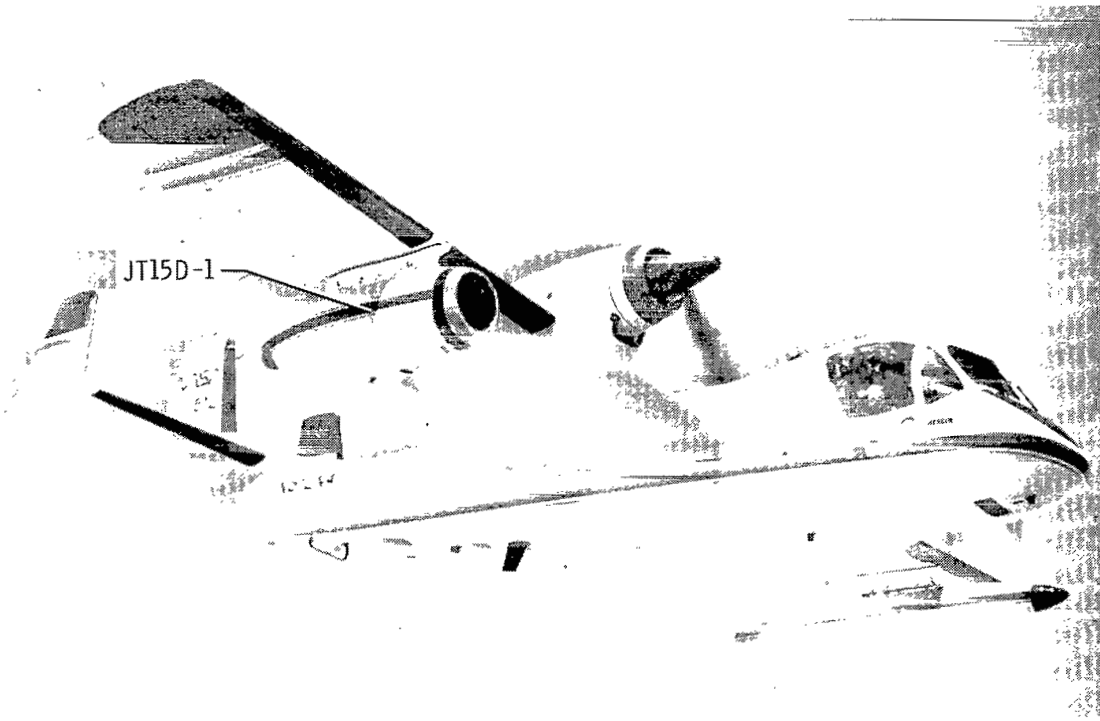
JT15D-1

L-80-3768.1

Figure 5.- JT15D-1 engine mounted on test aircraft in flight.

Transducer housing — — Epoxy fillet
— RTV
0.014 in.

Epoxy — — Pressure-sensitive diaphragm
with 0.0009-in. RTV overcoat

(a) Transducer mounting.

Optical
sensor
pulse

Tape
recorder

Signal
conditioner

Rotor-blade-
position pulse

Stator-vane-
mounted
transducers

Signal
conditioner

Aircraft
instrument
bay
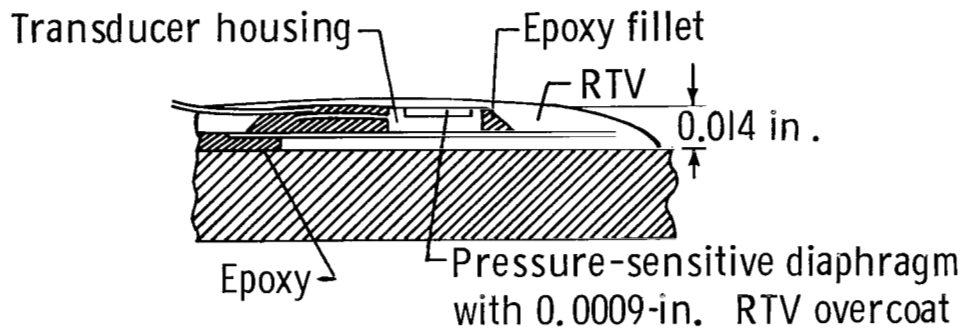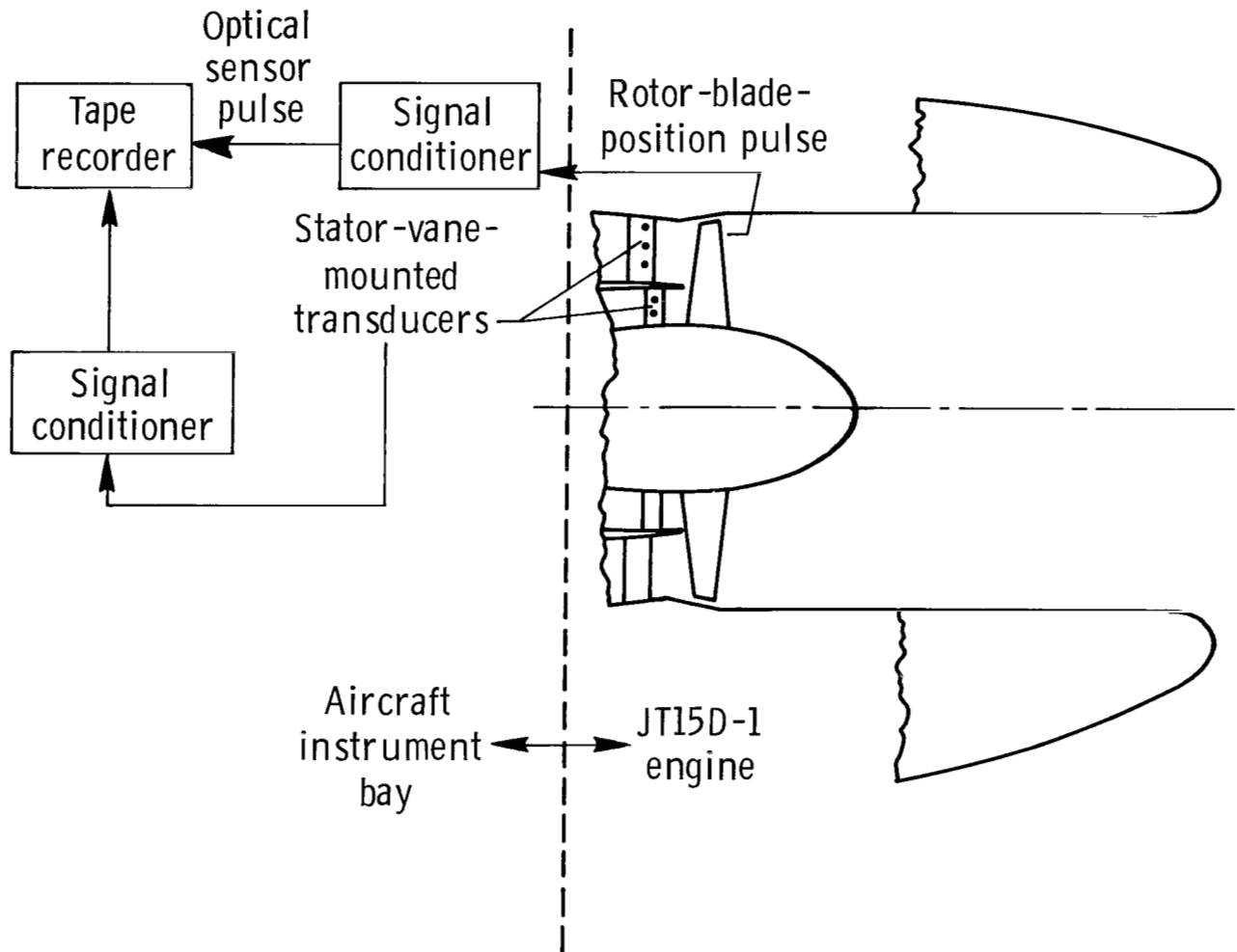
JT15D-1
engine

(b) Sketch of stator-vane-mounted transducer data system in JT15D-1 engine.

Figure 6.- Transducer-mounting technique and sketch of data-acquisition system.
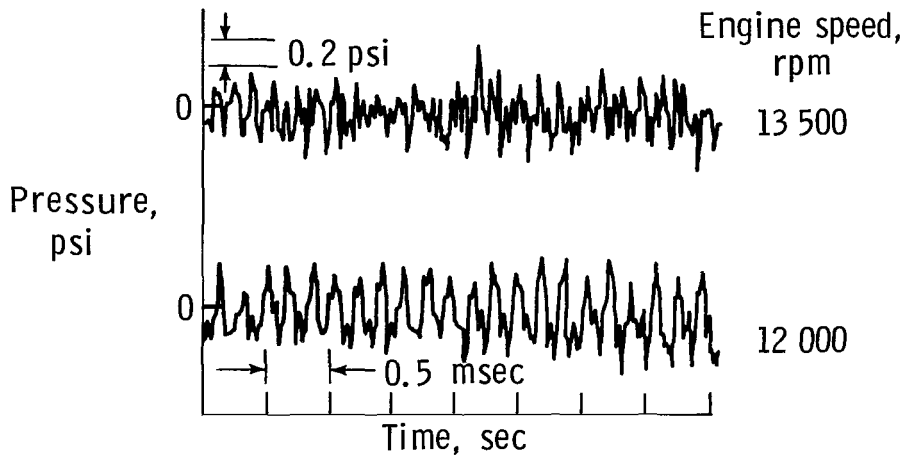
(a) Unenhanced average pressure time traces.
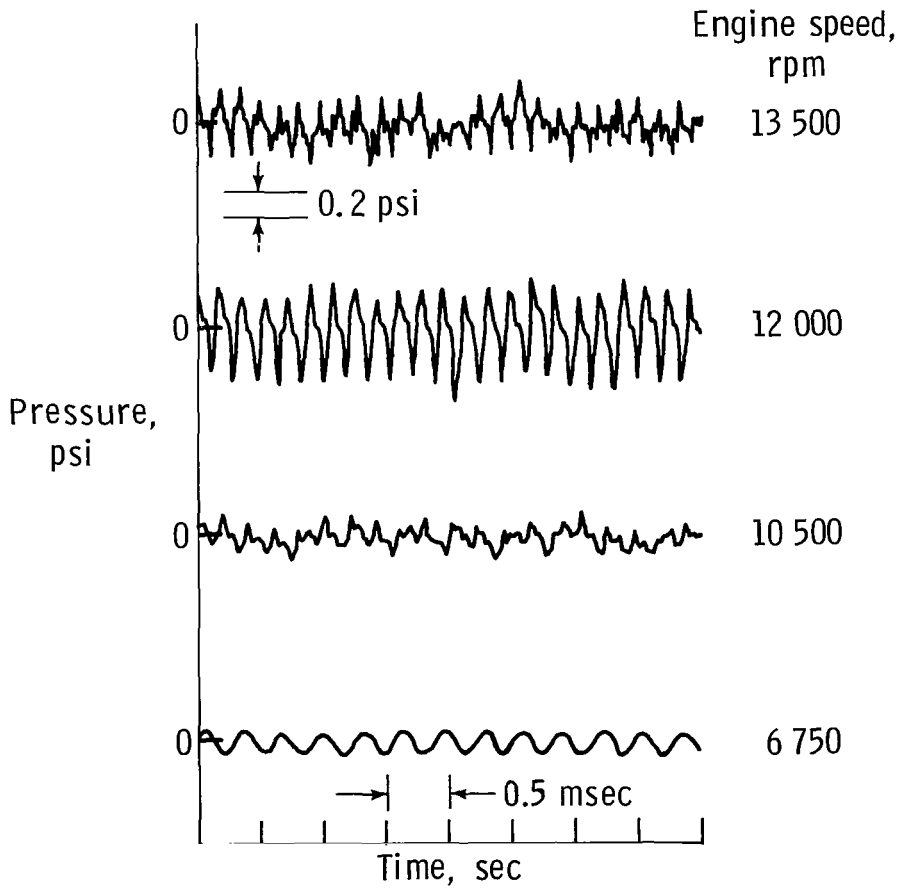
(b) Signal-enhanced pressure time traces.

Figure 7.- Comparison of unenhanced average pressure and
signal-enhanced pressure time traces for constant stator
location D for different static-test engine speeds.
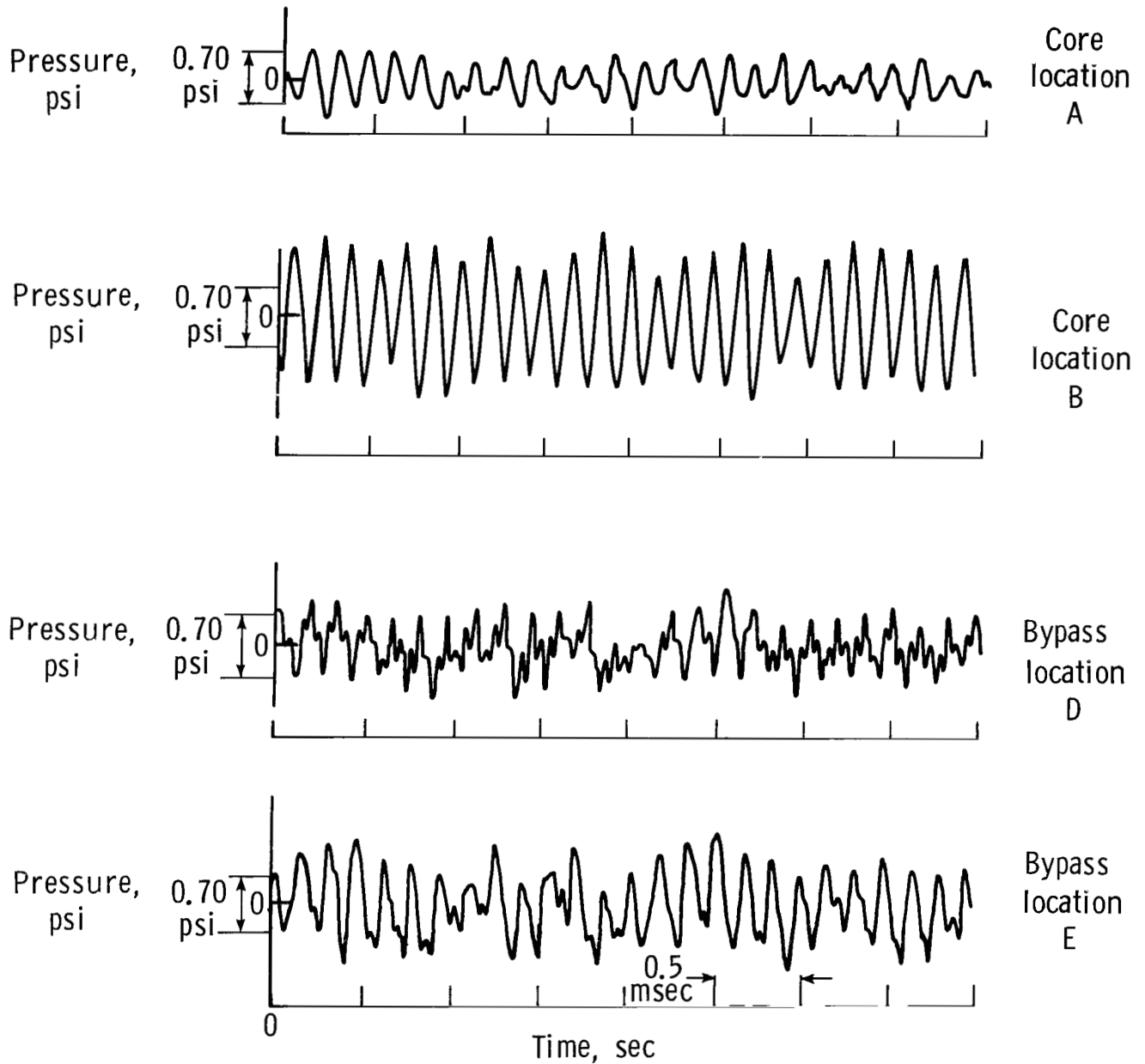
Figure 8.- Comparison of signal-enhanced pressure time traces at core- and bypass-stator locations for static-test constant engine speed of 13 500 rpm.
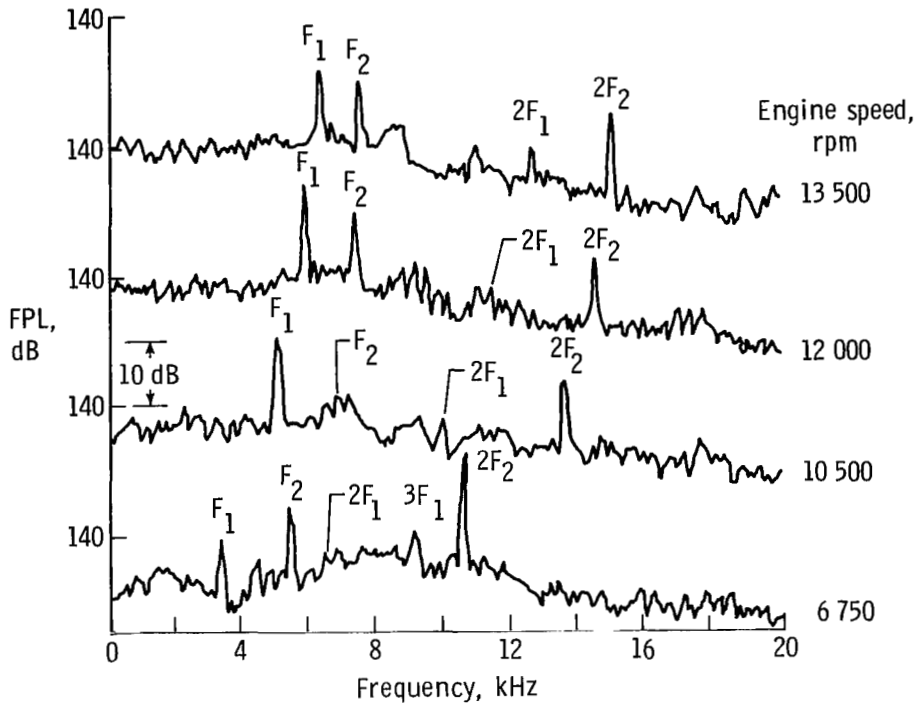
(a) Location A.
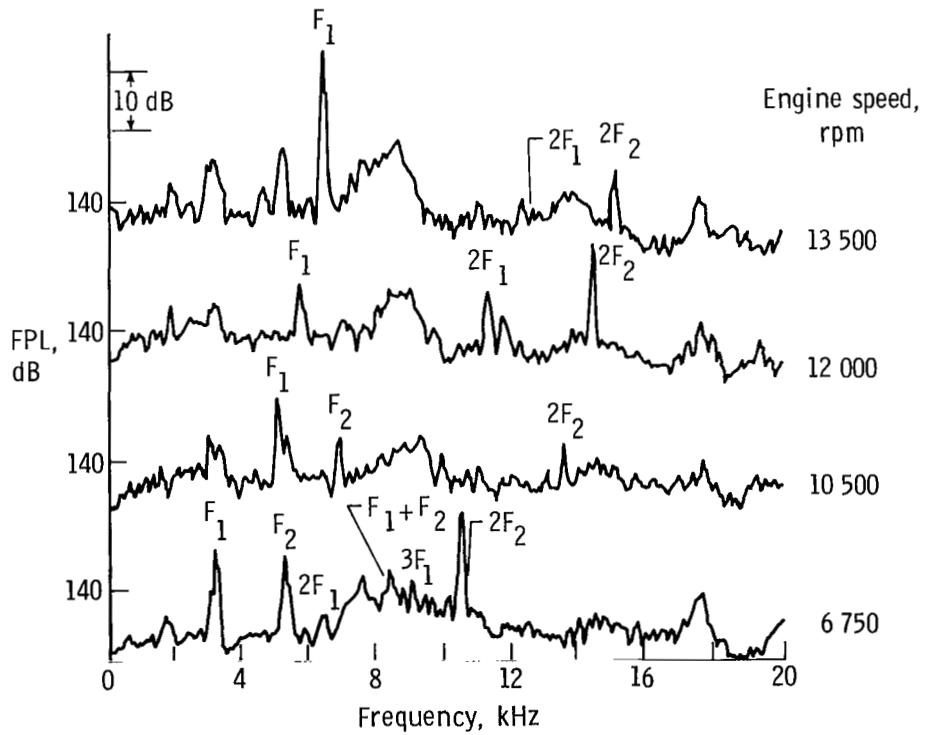
(b) Location B.

Figure 9.- Comparison of narrow-band (50 Hz) fluctuating pressure spectra of core-stator vanes for static-test engine speeds.
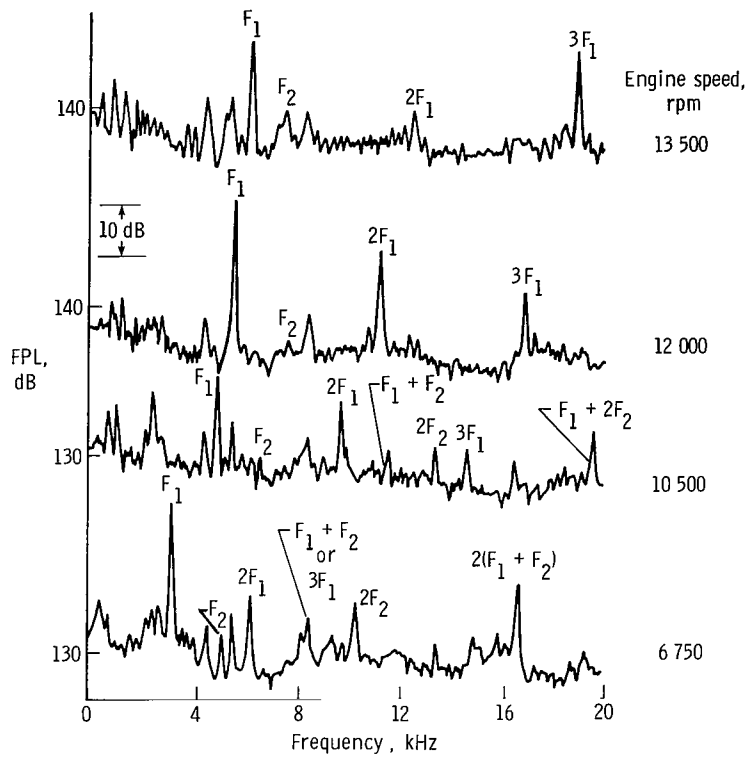
(a) Location D.
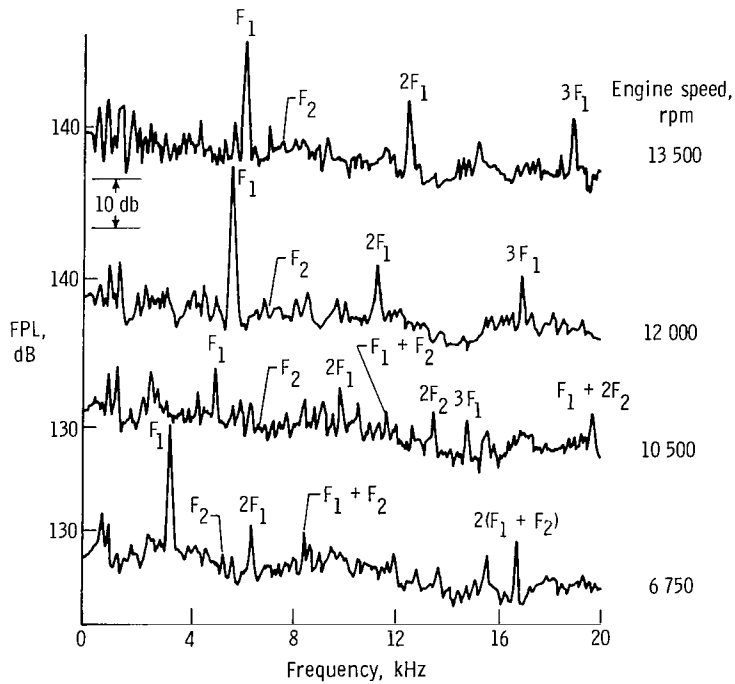
(b) Location E.

Figure 10.- Comparison of narrow-band (50 Hz)
fluctuating pressure spectra of bypass-stator
vanes for static-test engine speeds.

(a) Core stator.

170

160

FPL,
dB 150

140

130

120

Location
○ A ● } Broadband
□ B ■

6   8   10   12   14×10³

Engine speed, rpm

(b) Bypass stator.

170

160

FPL,
dB 150

140

130

120

110

Location
○ D ● } Broadband
□ E ■

6   8   10   12   14 ×10³
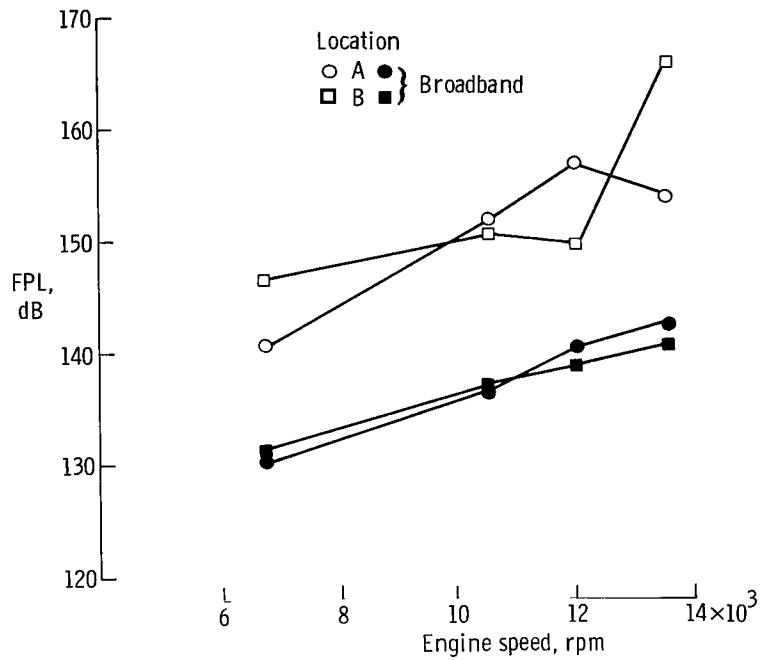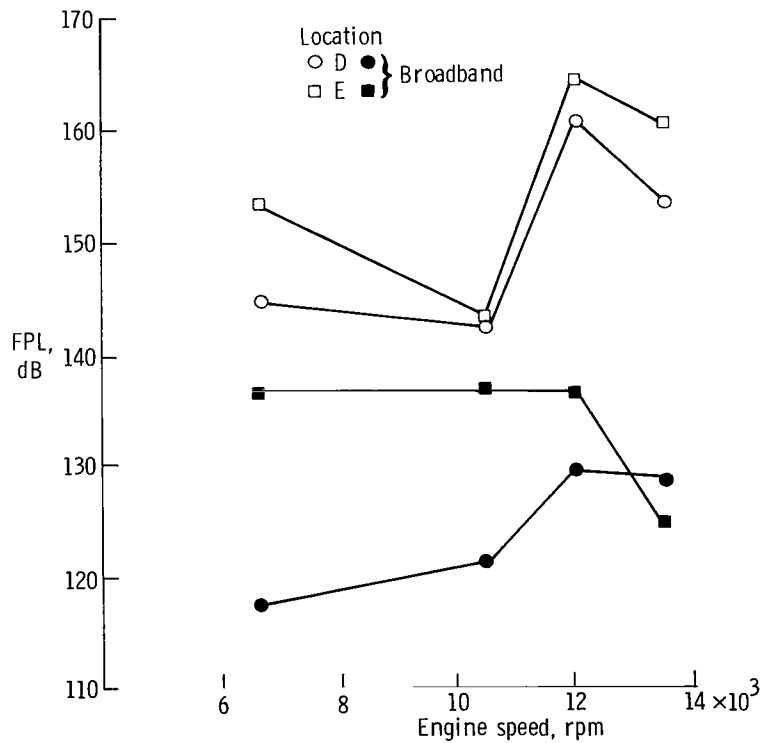
Engine speed, rpm

Figure 11.- Stator-vane narrow-band (50 Hz) fluctuating
pressure levels measured at fan-rotor F_1 BPF tone for
static-test engine speeds.
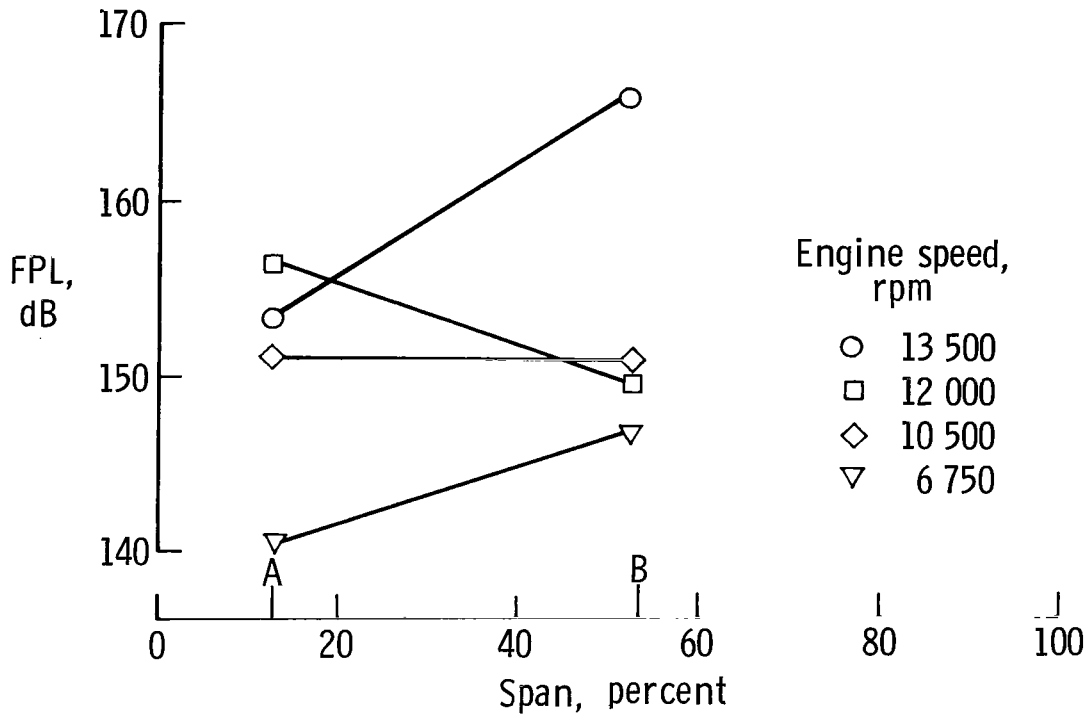
(a) Core stator. Span length, 1.9 in.
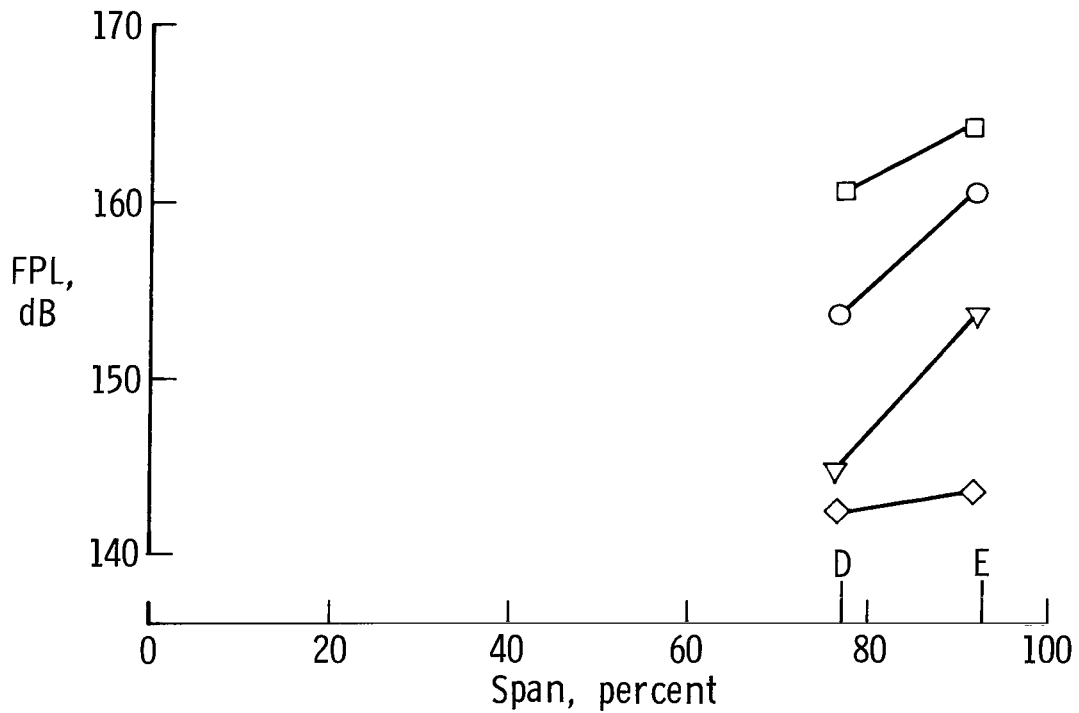
(b) Bypass stator. Span length, 3.3 in.

Figure 12.- Spanwise distribution of measured narrow-band (50 Hz) fluctuating
pressure levels of fan-rotor F_1 BPF tone for static-test engine speeds.
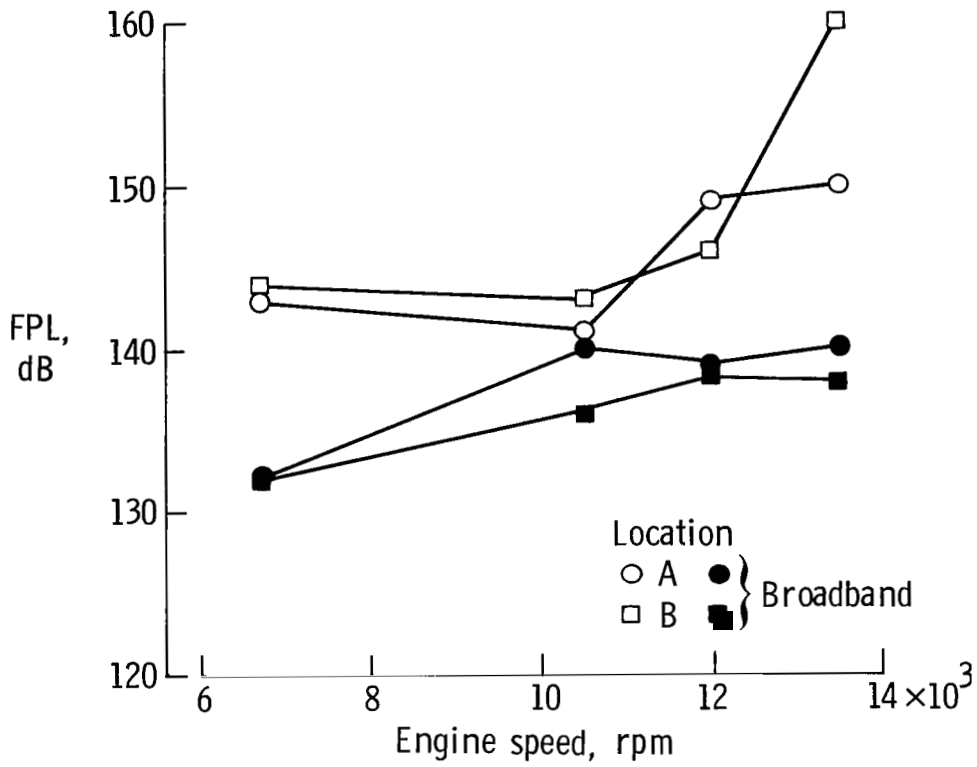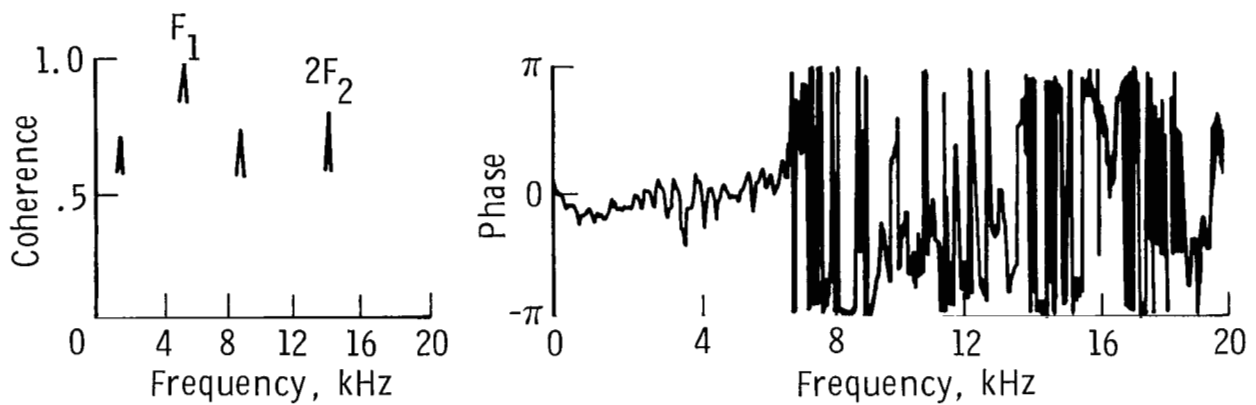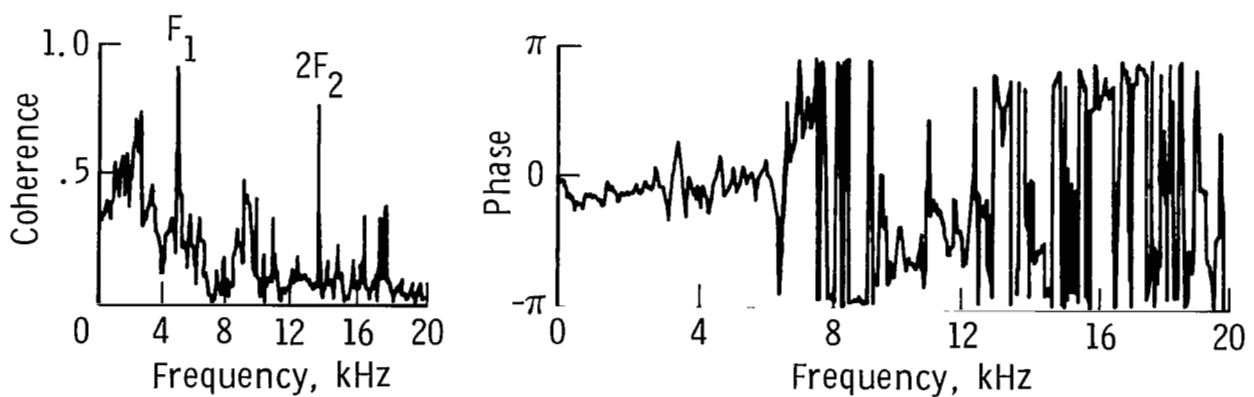
(a) Core stator.
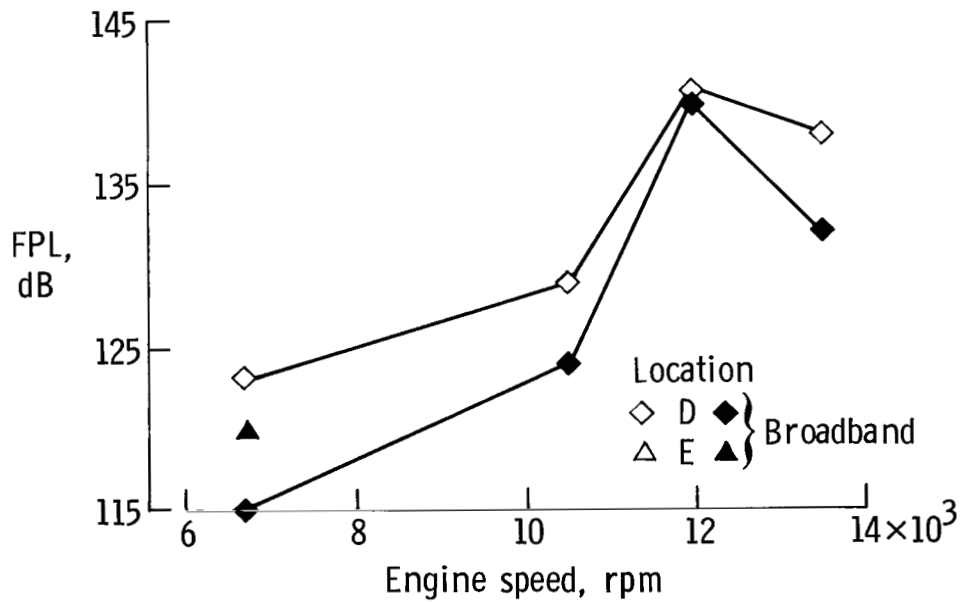
(b) Bypass stator.

Figure 13.- Comparison of measured narrow-band (50 Hz) fluctuating pressure levels for core and bypass stators at core-compressor F_2 BPF tones for static-test engine speeds.
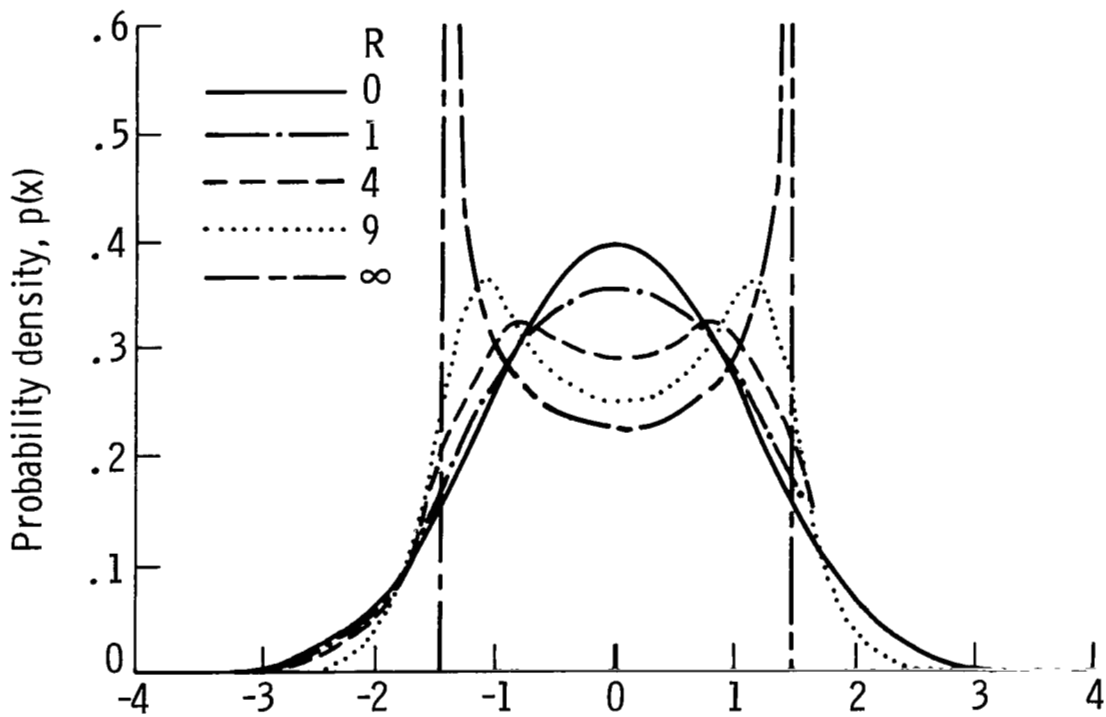
Figure 14.- Probability density functions of sine signal in Gaussian noise.
(See ref. 27.) $R = \sigma_s^2/\sigma_n^2$.
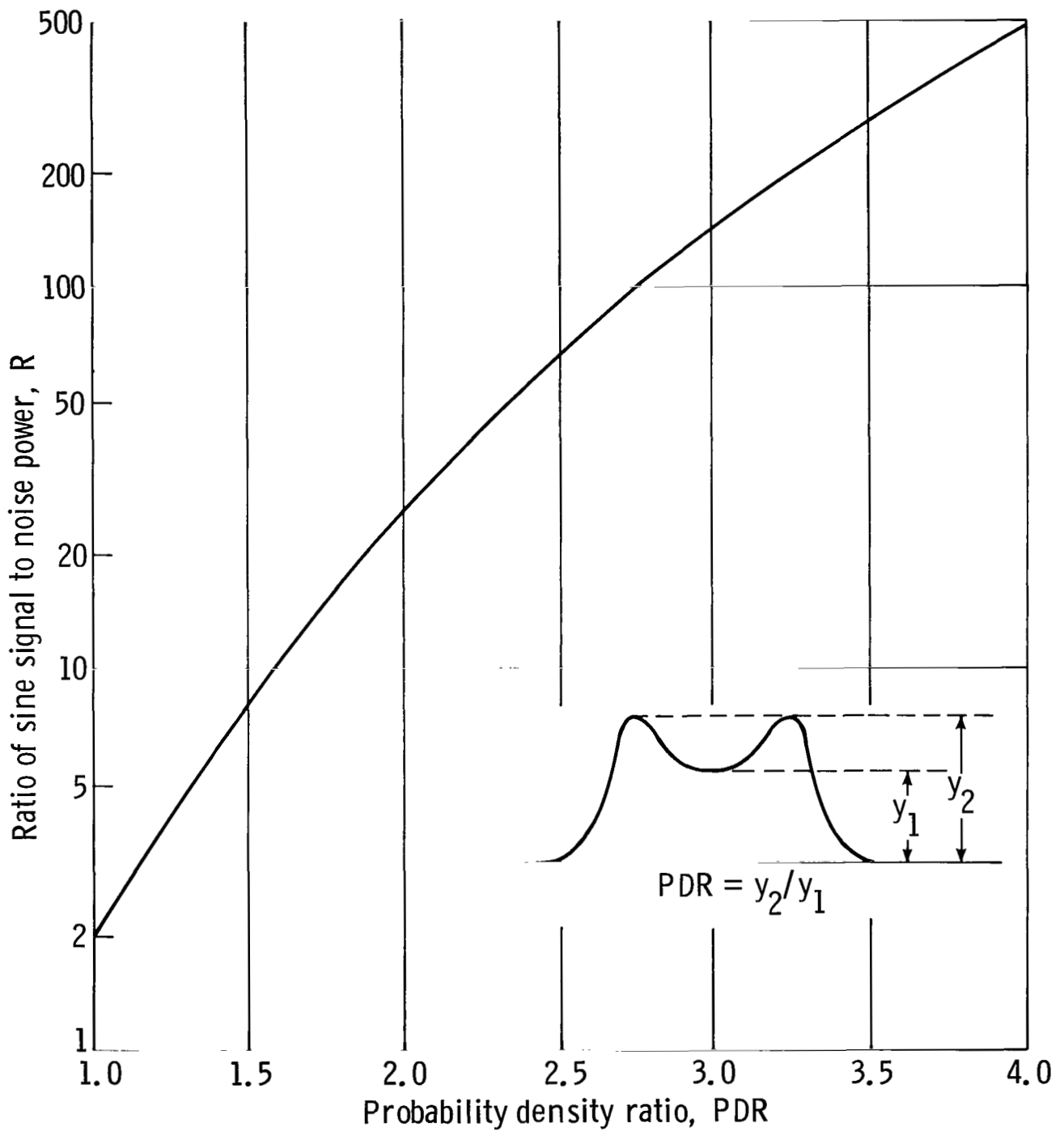
Figure 15.- Ratio of sine signal to noise power as a function of probability density ratio. (See ref. 28.) $R = \sigma_s^2/\sigma_n^2$.

Probability density, p(x)

1.0

.5

0

-4   -2   0   2   4

y_1 y_2
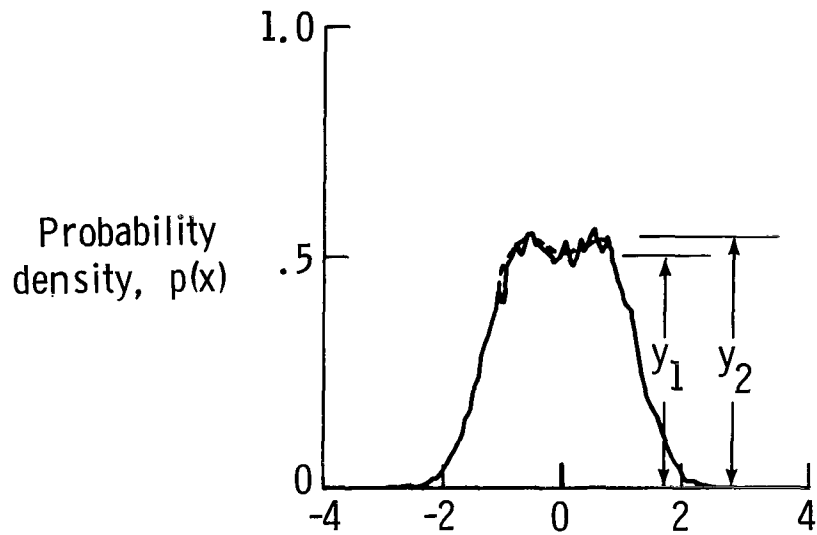
(a) PDF for location A for static-test engine speed of 13 500 rpm. PDR = y_2/y_1 = 1.1.

Probability density, p(x)

1.0

.5

0

-2   0   2   4

y_1 y_2
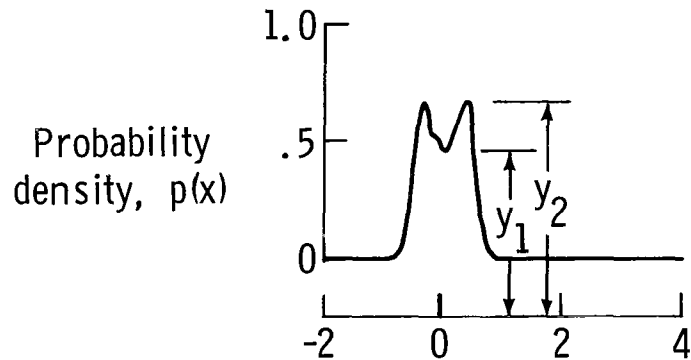
(b) PDF for location A for static-test engine speed of 12 000 rpm. PDR = y_2/y_1 = 1.5.

Figure 16.- Examples typical of measured probability density function and PDR of amplitudes of fan-rotor F_1 BPF tone.
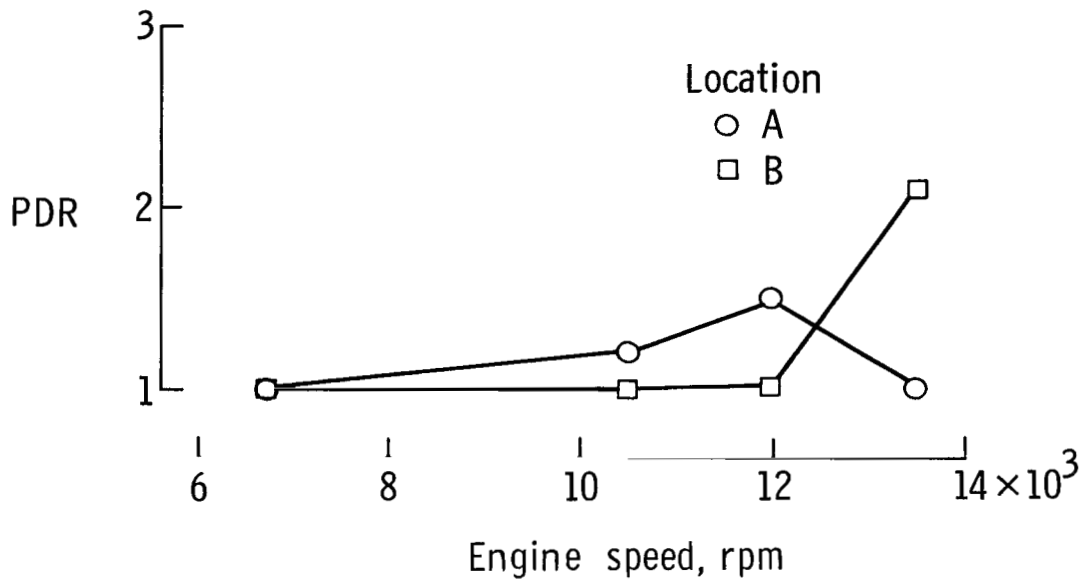
(a) Core stator.
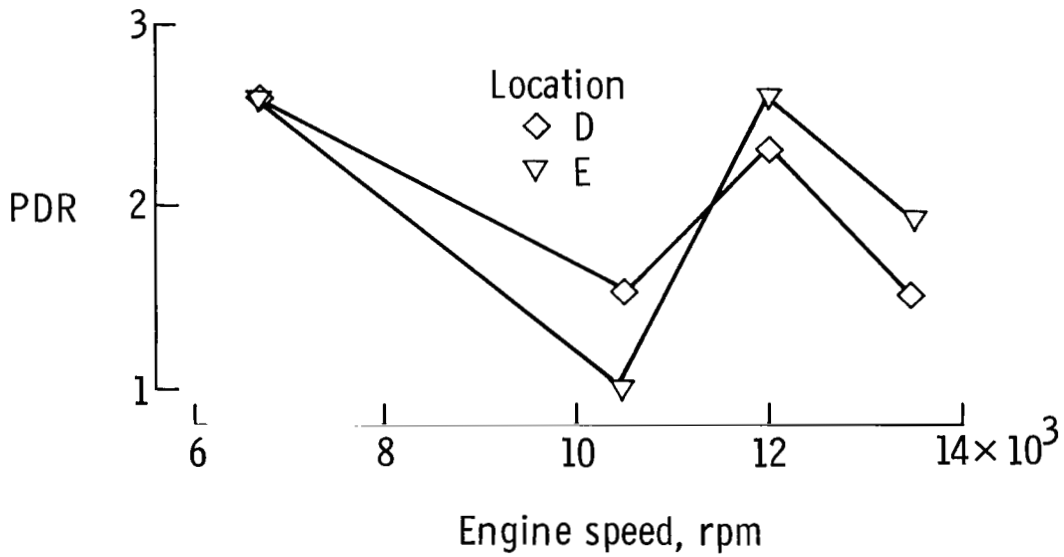
(b) Bypass stator.

Figure 17.- Comparison of probability density ratios of fluctuating pressures of F_1 BPF tones as measured at stator locations for static-test engine speeds.
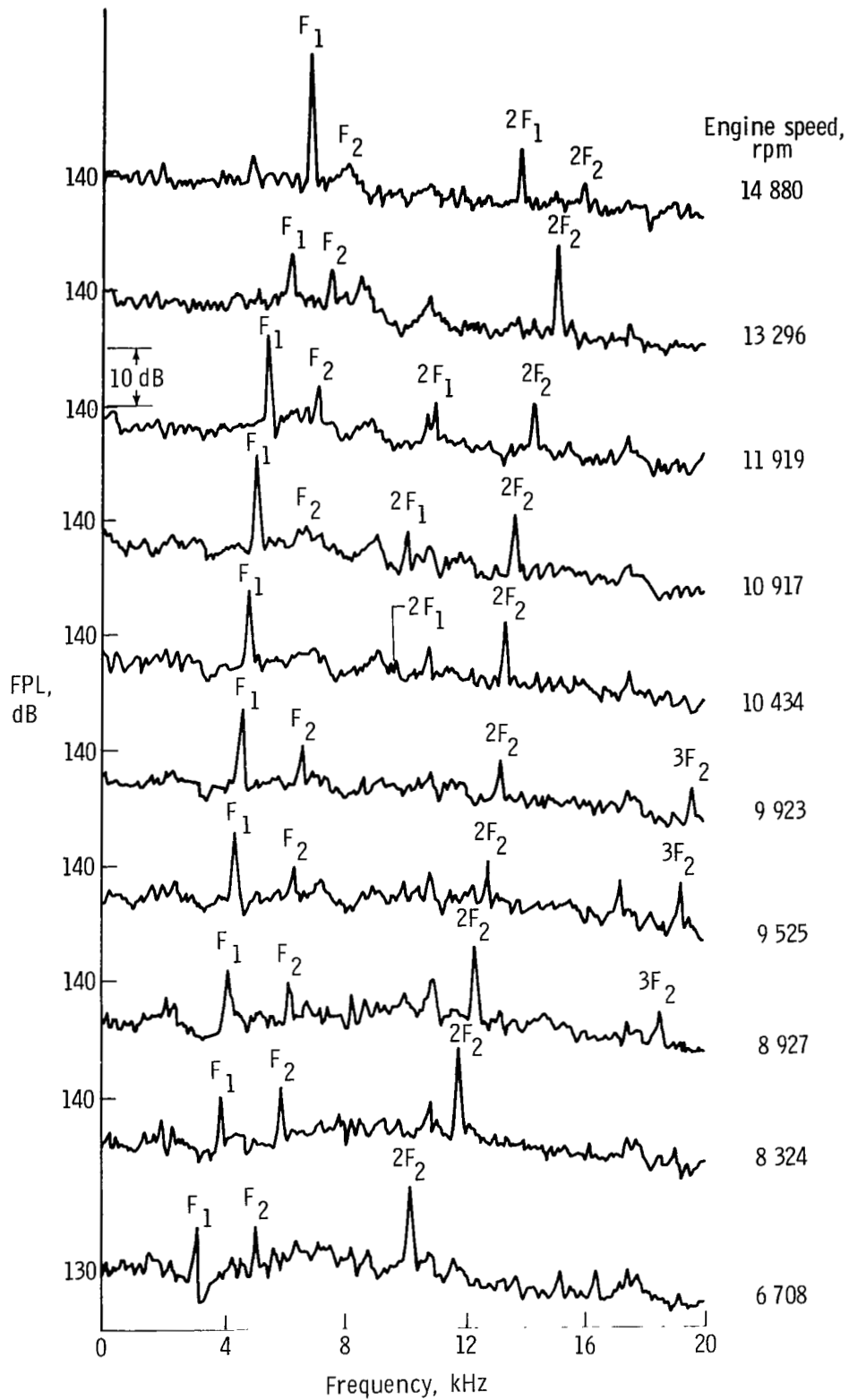
(a) Location A.

Figure 18.- Comparison of narrow-band (50 Hz) fluctuating pressure spectra of stator vanes for flight-test engine speeds.
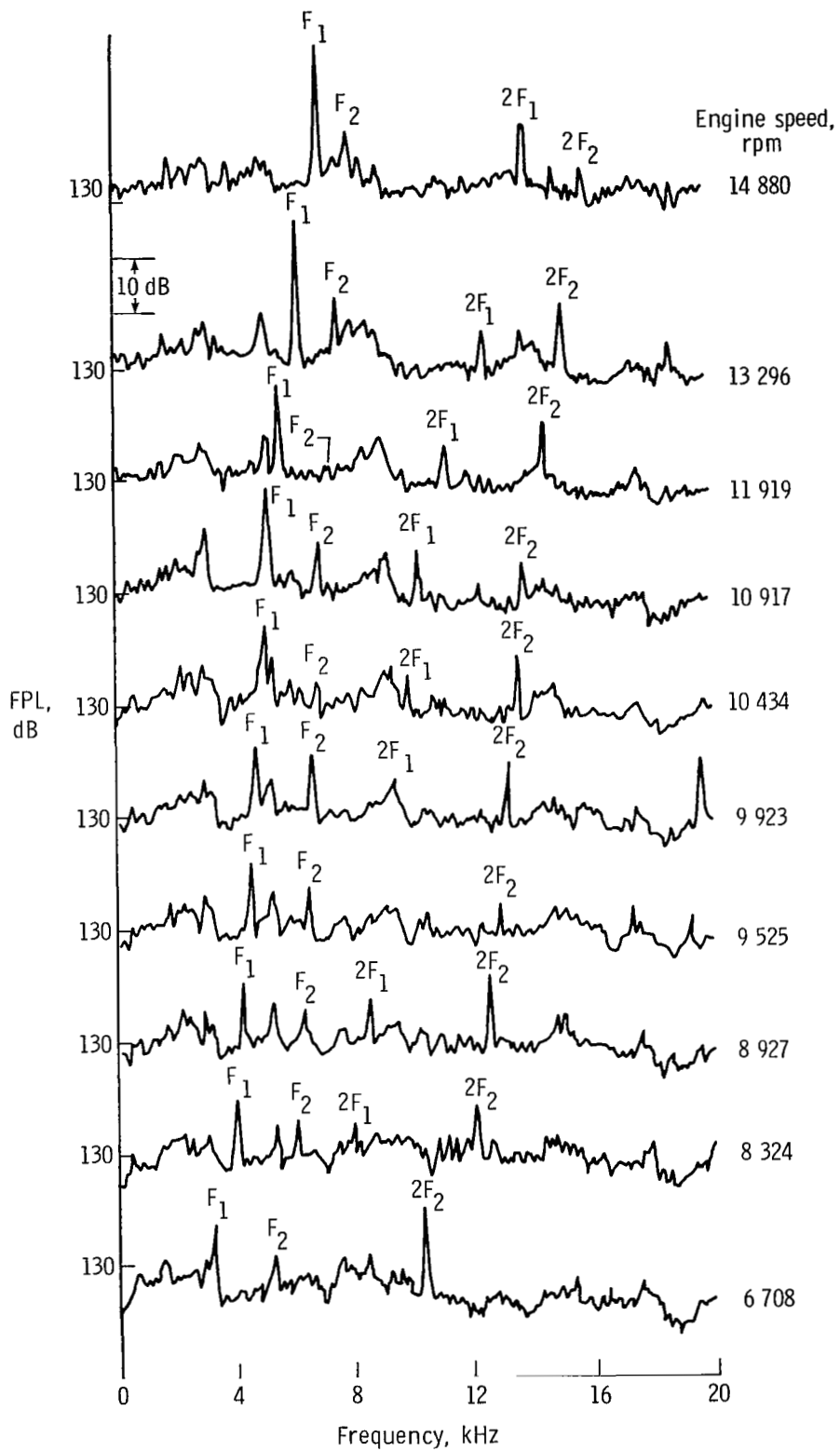
(b) Location B.

Figure 18.- Continued.
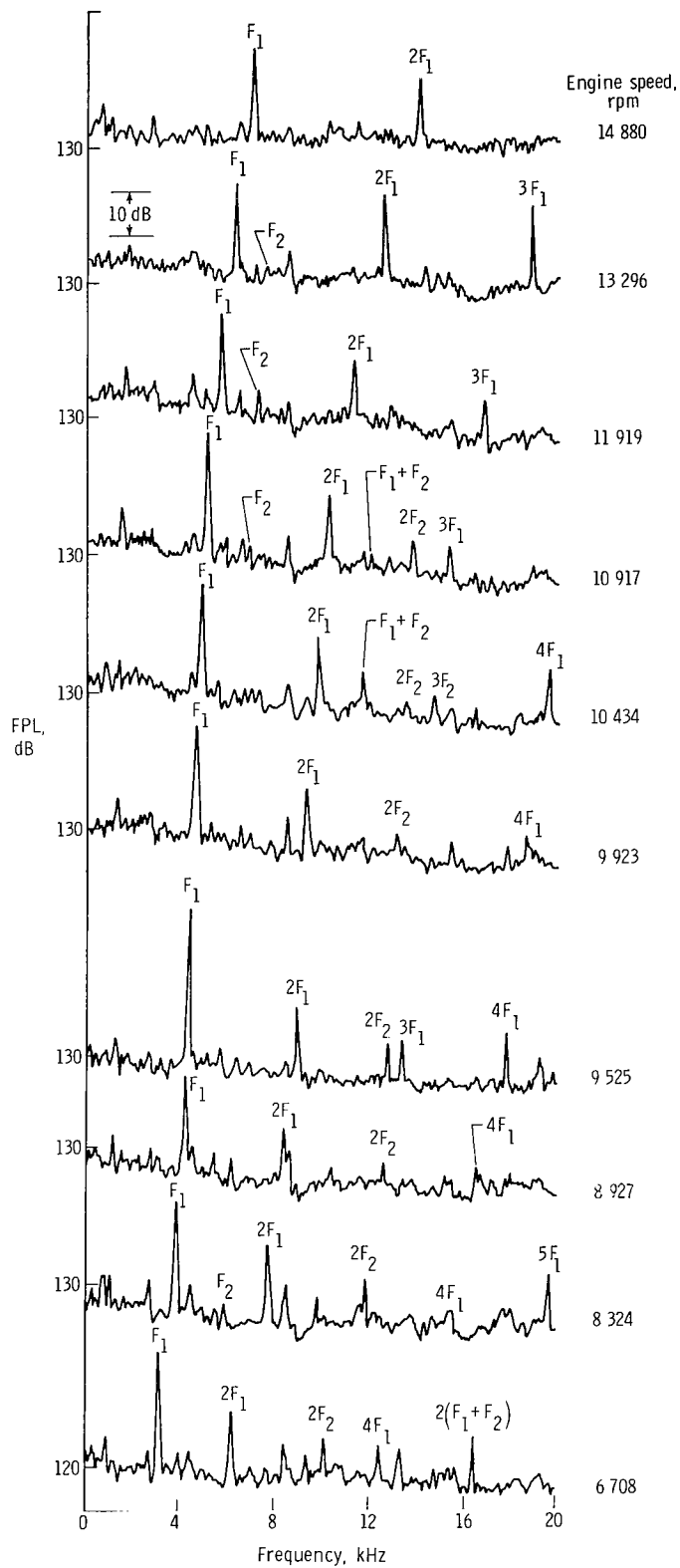
(c) Location C.

Figure 18.- Continued.
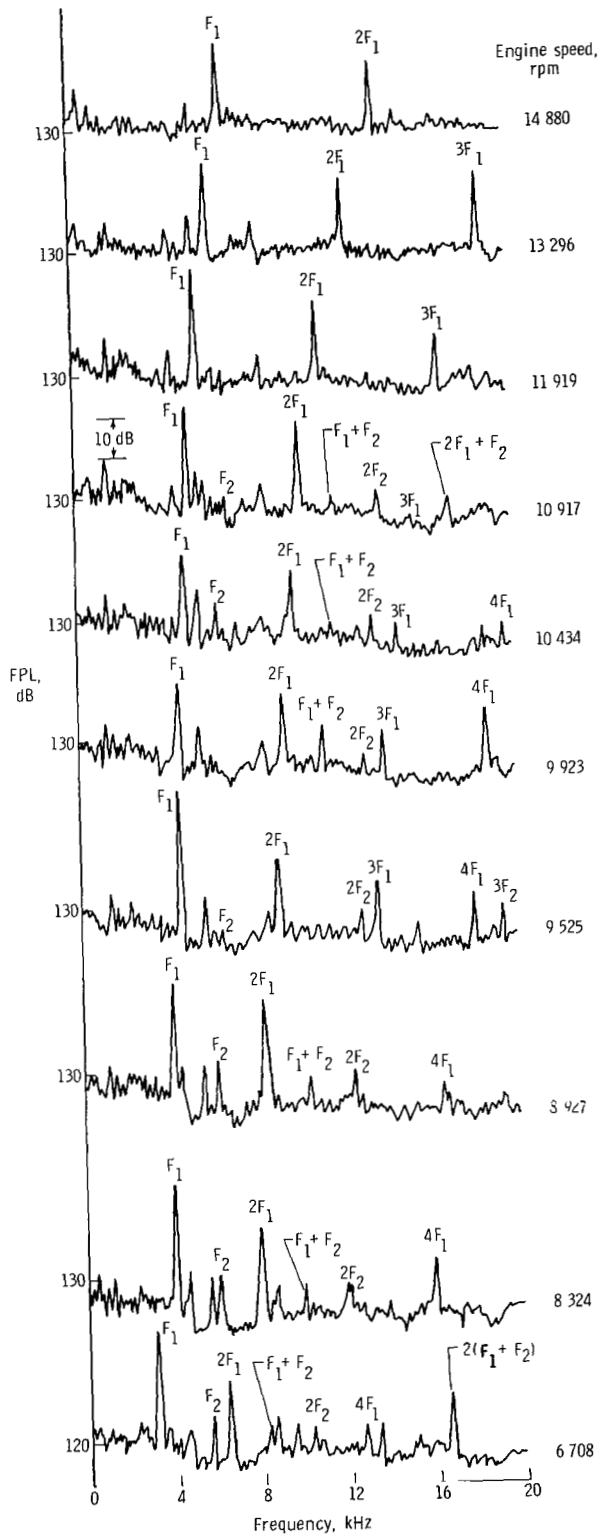
(d) Location D.

Figure 18.- Continued.
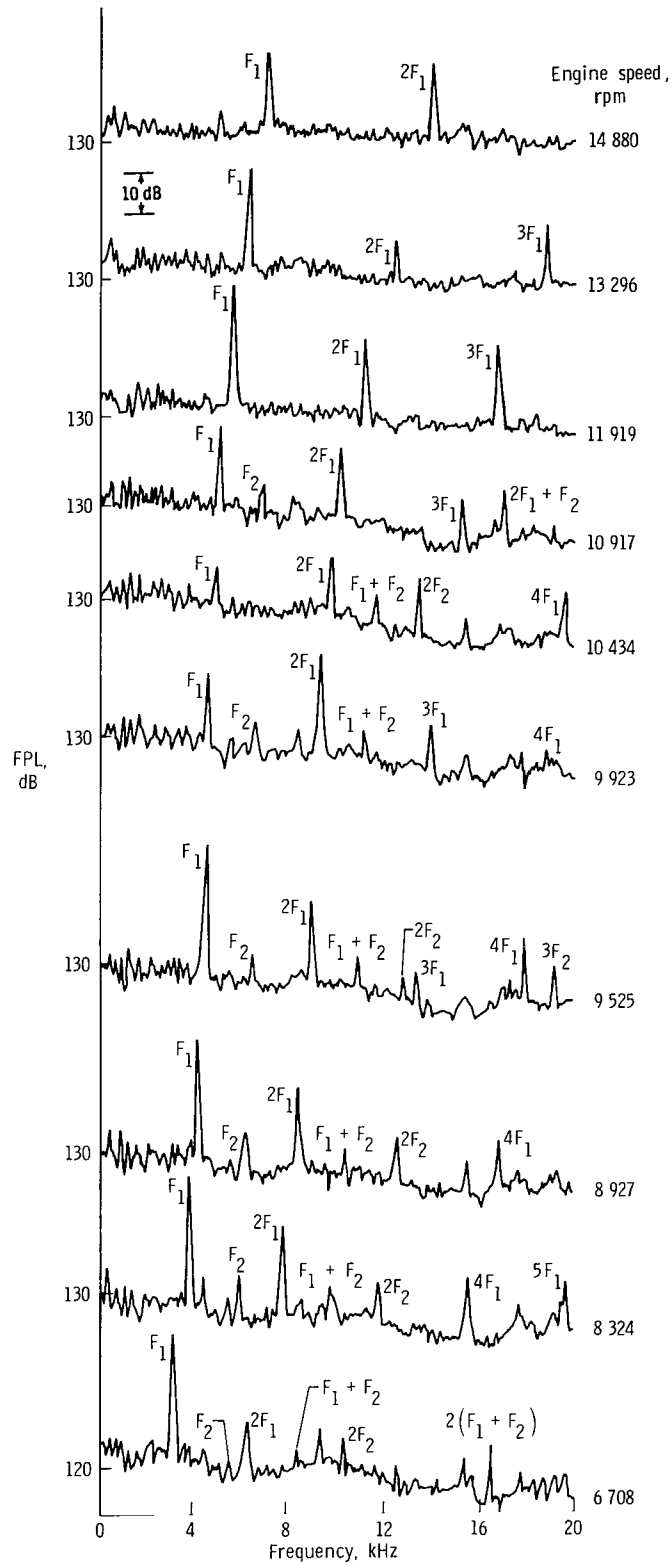
(e) Location E.

Figure 18.- Concluded.
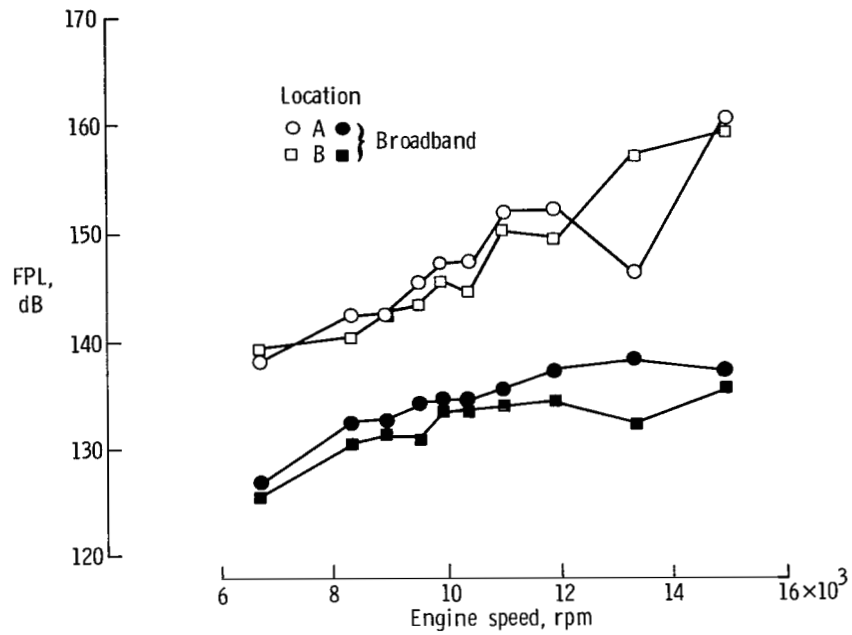
(a) Core stator.
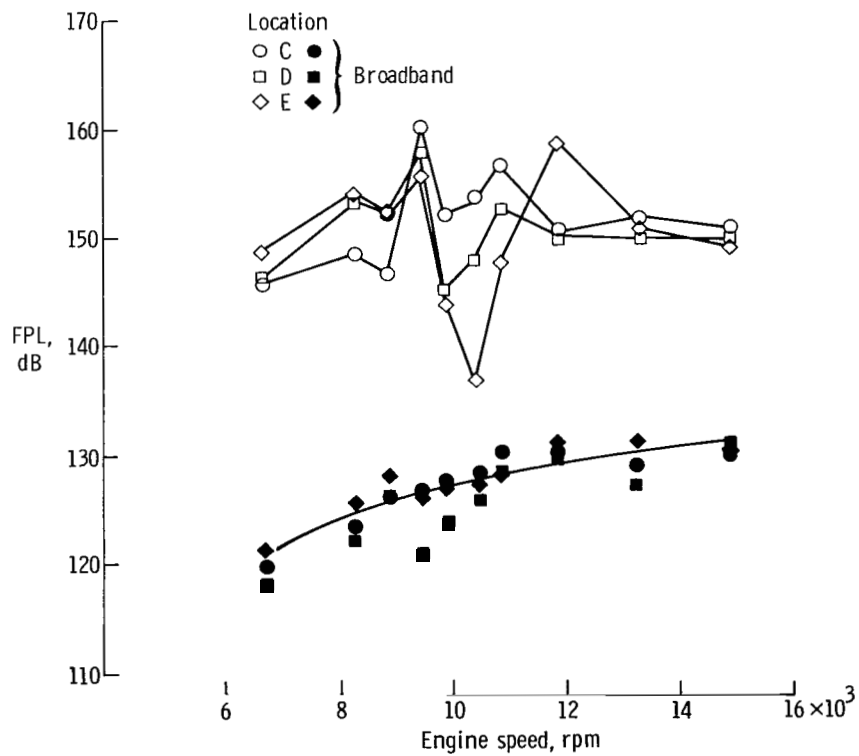
(b) Bypass stator.

Figure 19.- Stator-vane narrow-band (50 Hz) fluctuating pressure levels measured at fan-rotor F_1 BPF tone for flight-test engine speeds.
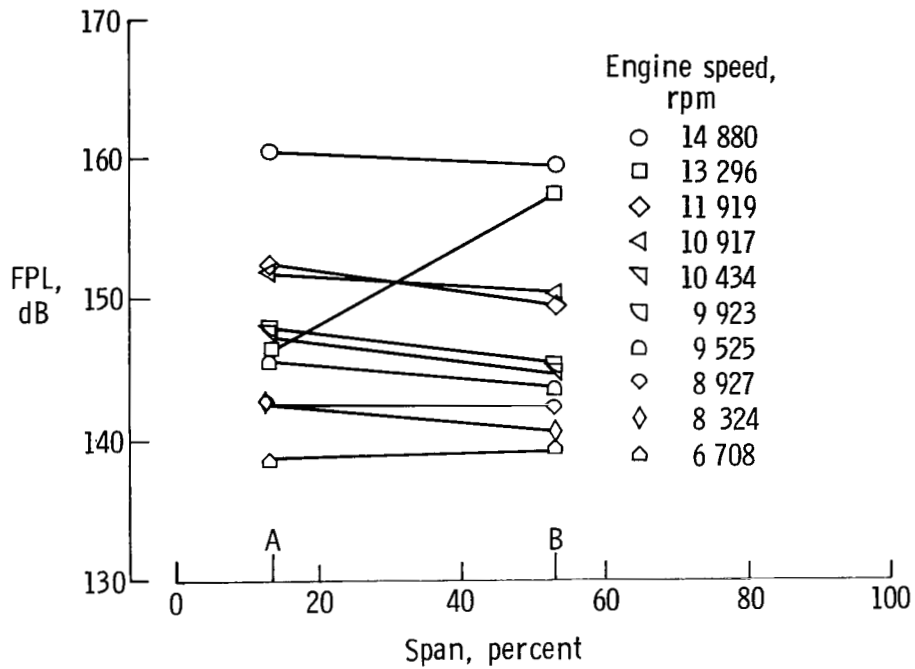
Figure 20.- Spanwise distribution of core-stator narrow-band (50 Hz) fluctuating pressure levels measured at fan-rotor F_1 BPF tones for flight-test engine speeds. (Span length, 1.9 in.)
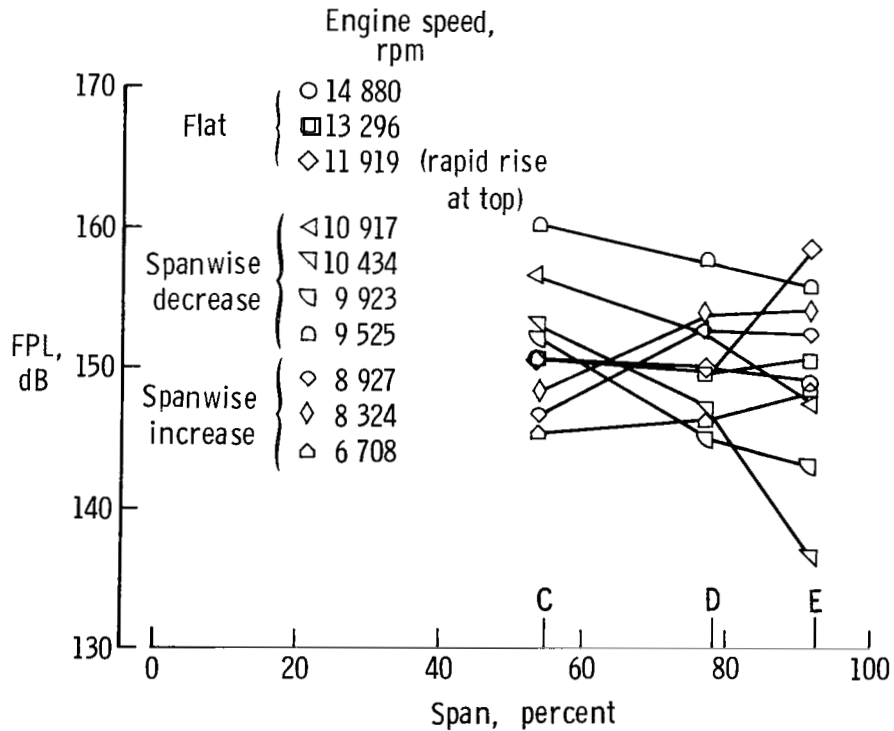
Figure 21.- Spanwise distribution of bypass-stator narrow-band (50 Hz) fluctuating pressure levels measured at fan-rotor F_1 BPF tones for flight-test engine speeds. (Span length, 3.3 in.)
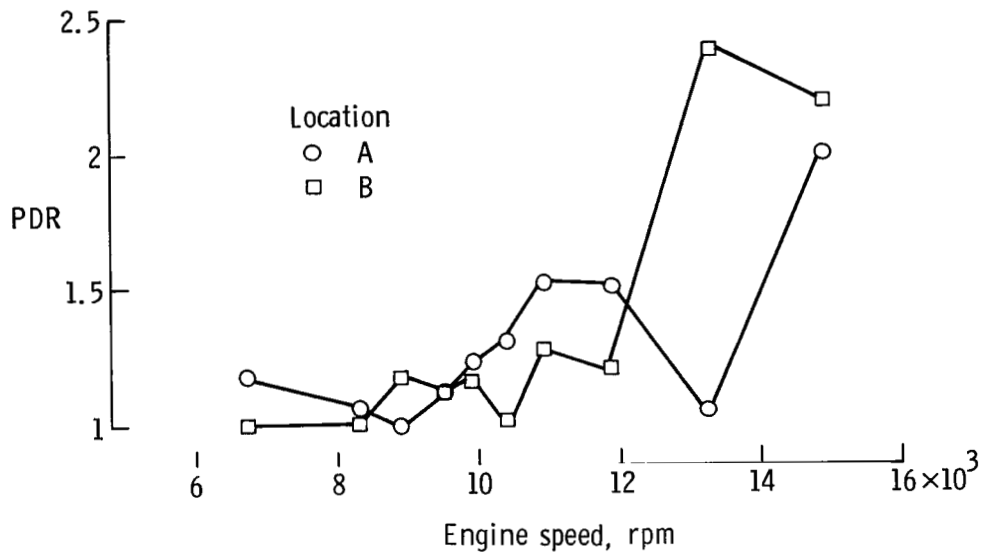
(a) Core stator.
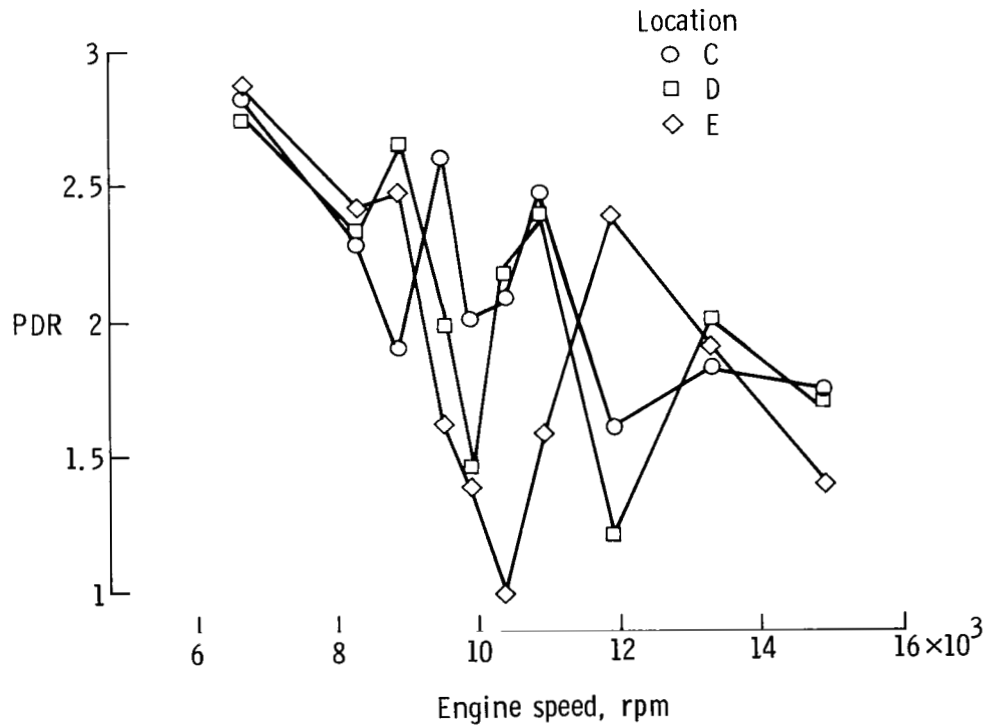
(b) Bypass stator.

Figure 22.- Comparison of probability density ratios of fluctuating pressures of F_1 BPF tones as measured at stator locations for flight-test engine speeds.
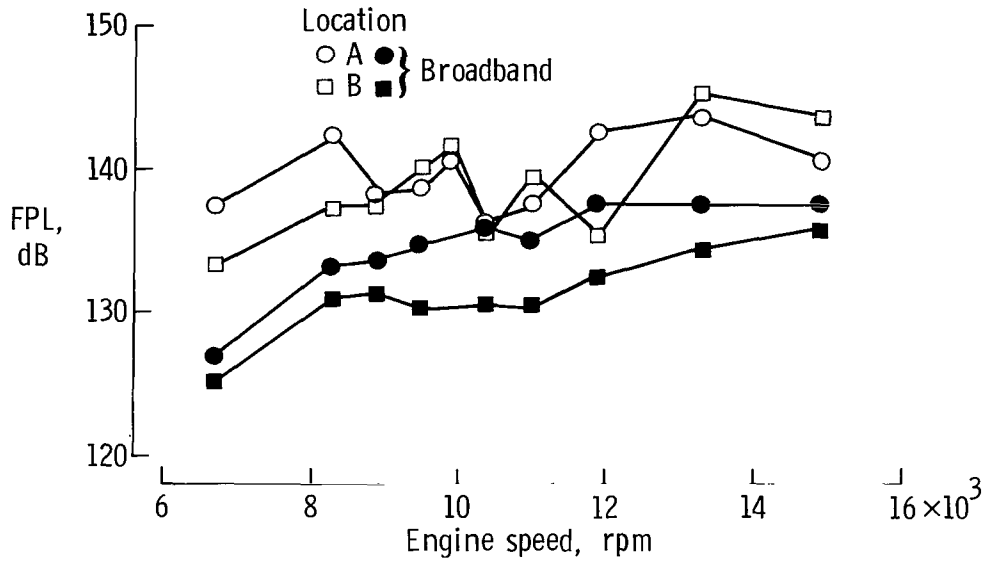
(a) Core stator.
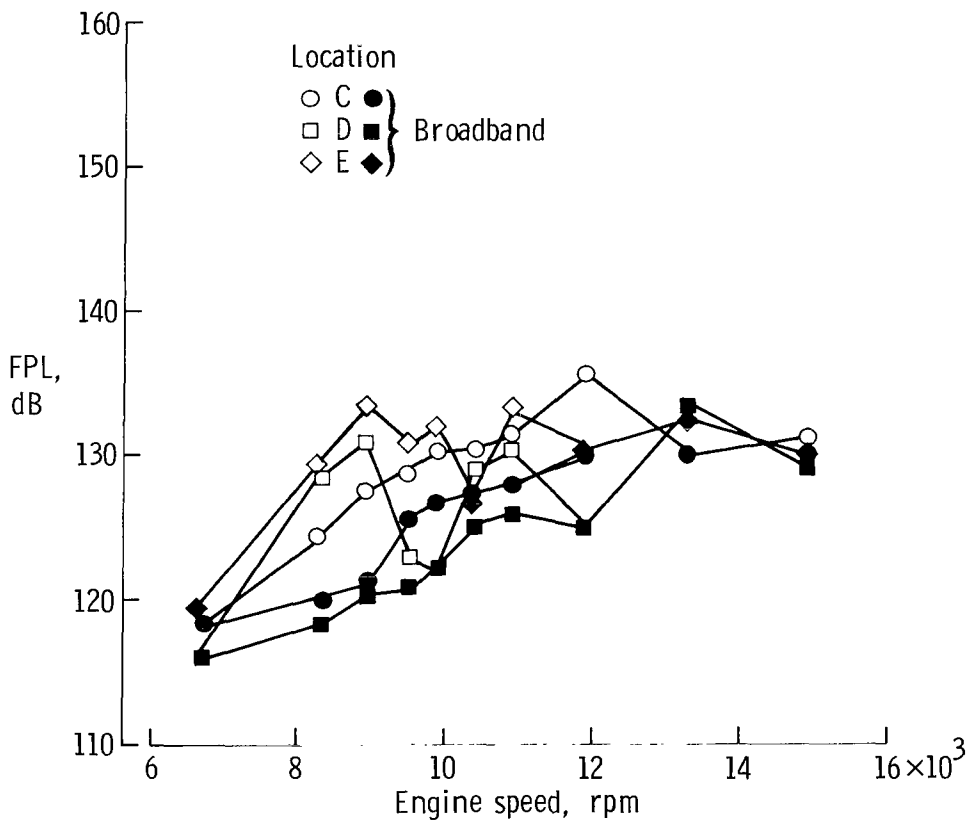
(b) Bypass stator.

Figure 23.- Comparison of measured narrow-band (50 Hz) fluctuating
pressure levels of core and bypass stators at core-compressor
F_2 BPF tones for flight-test engine speeds.
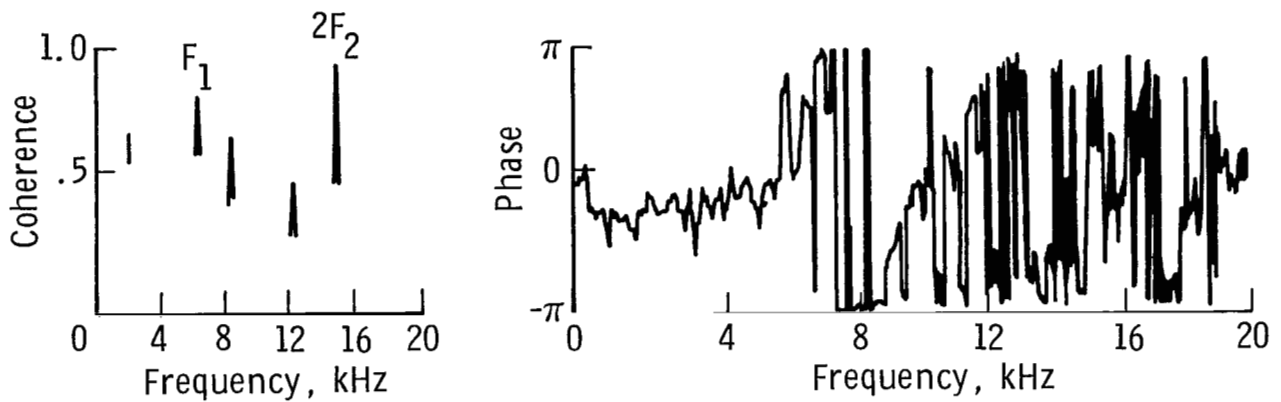
(a) Supersonic tip speed. Engine speed, 13 296 rpm.

(b) Transonic tip speed. Engine speed, 11 919 rpm.

(c) Subsonic tip speed. Engine speed, 10 434 rpm.

Figure 24.- Coherence and phase relationships between pressures measured at core-stator locations A and B at supersonic, transonic, and subsonic fan-rotor-blade tip speeds for flight tests.
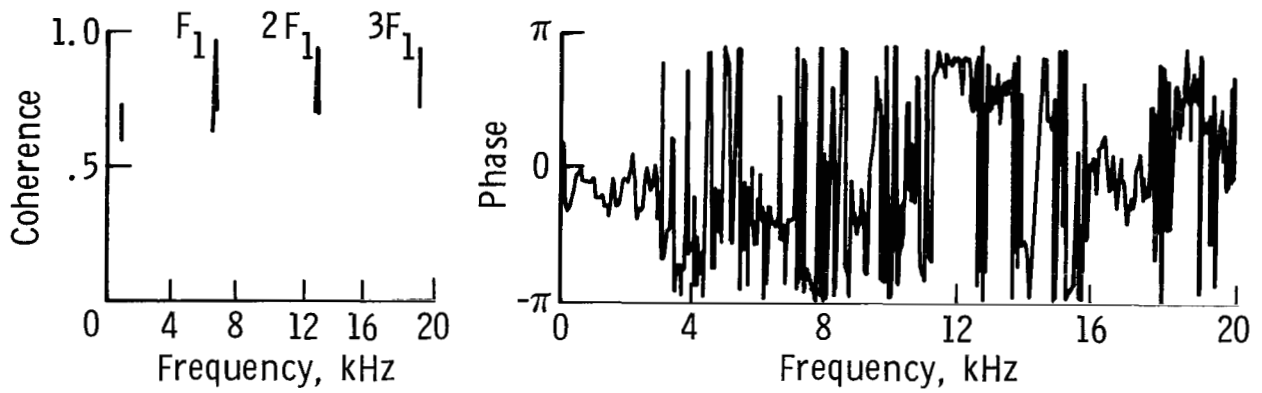
(a) Supersonic tip speed. Engine speed, 13 296 rpm.
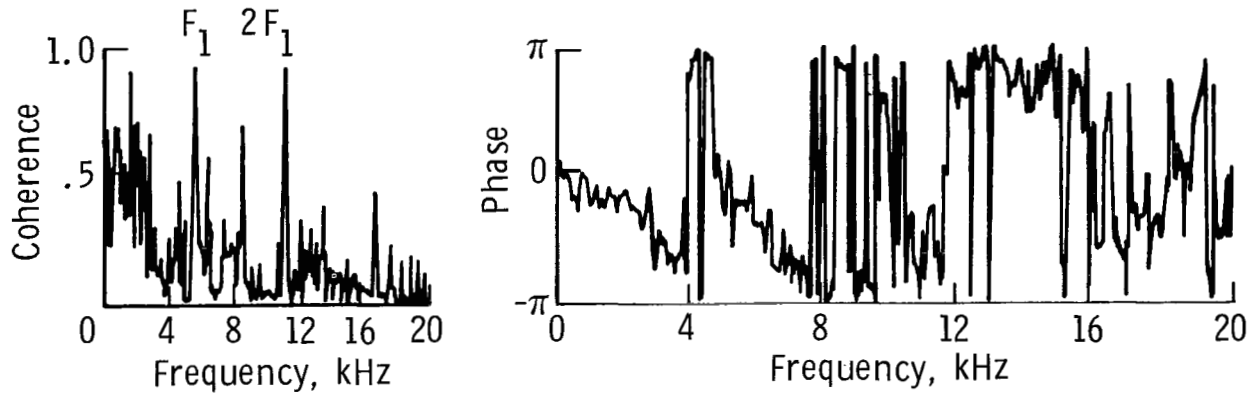
(b) Transonic tip speed. Engine speed, 11 919 rpm.
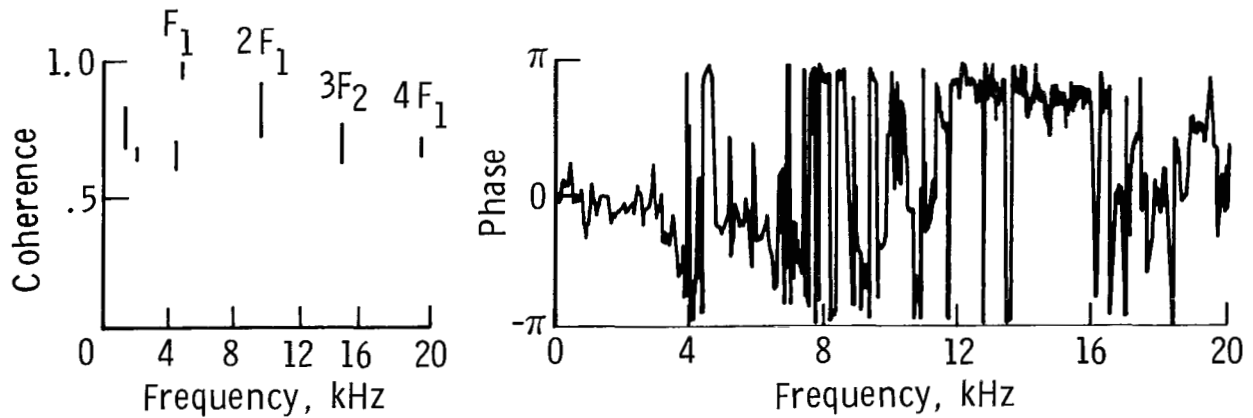
(c) Subsonic tip speed. Engine speed, 10 434 rpm.

Figure 25.- Coherence and phase relationships between pressures measured at bypass-stator locations C and D at supersonic, transonic, and subsonic fan-rotor-blade tip speeds for flight tests.
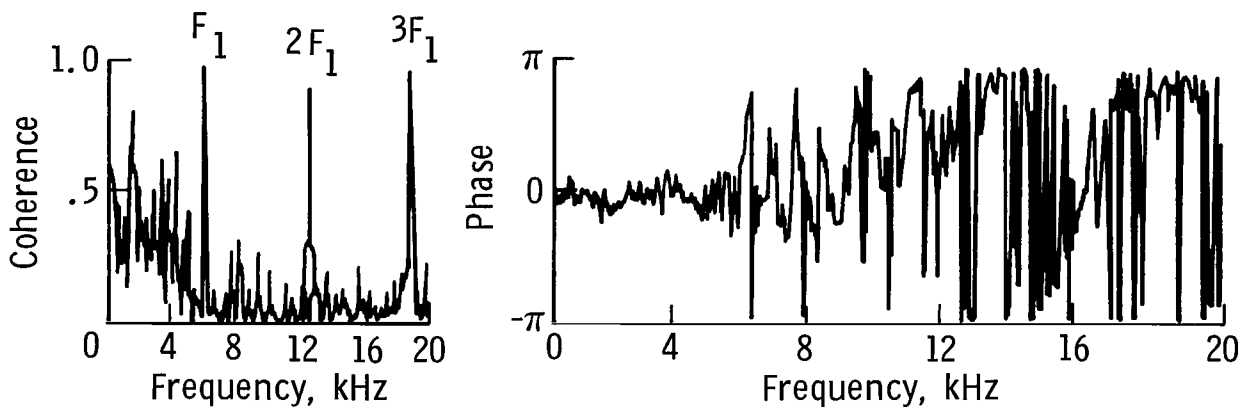
(a) Supersonic tip speed. Engine speed, 13 296 rpm.
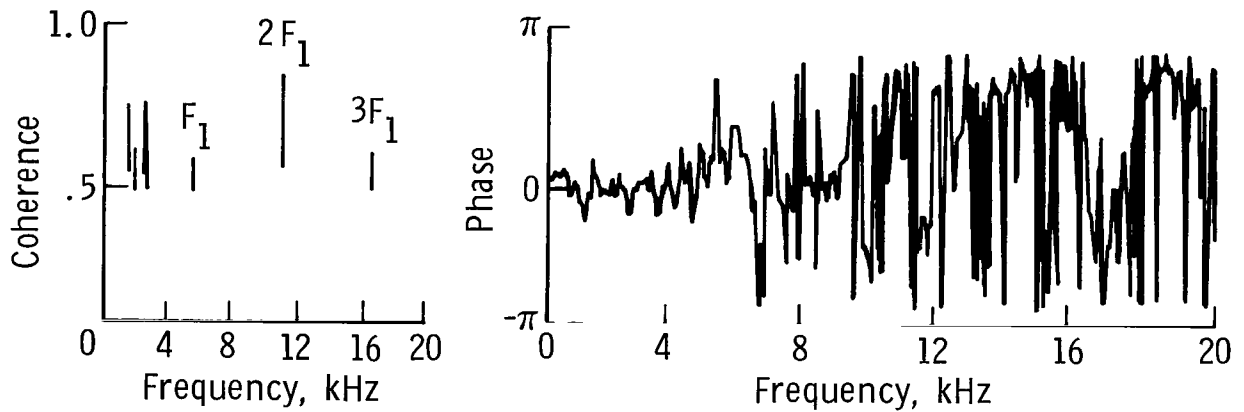
(b) Transonic tip speed. Engine speed, 11 919 rpm.
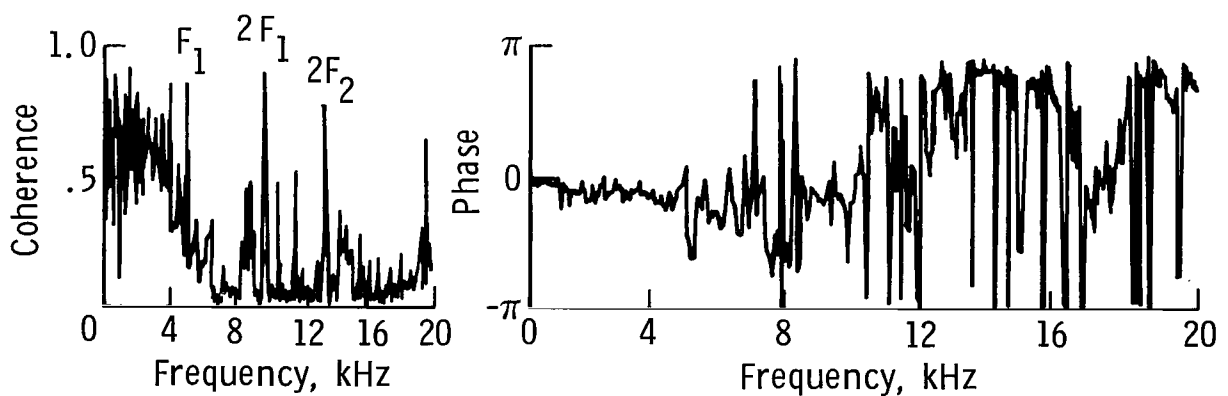
(c) Subsonic tip speed. Engine speed, 10 434 rpm.

Figure 26.- Coherence and phase relationships between pressures measured at bypass-stator locations D and E at supersonic, transonic, and subsonic fan-rotor-blade tip speeds for flight tests.
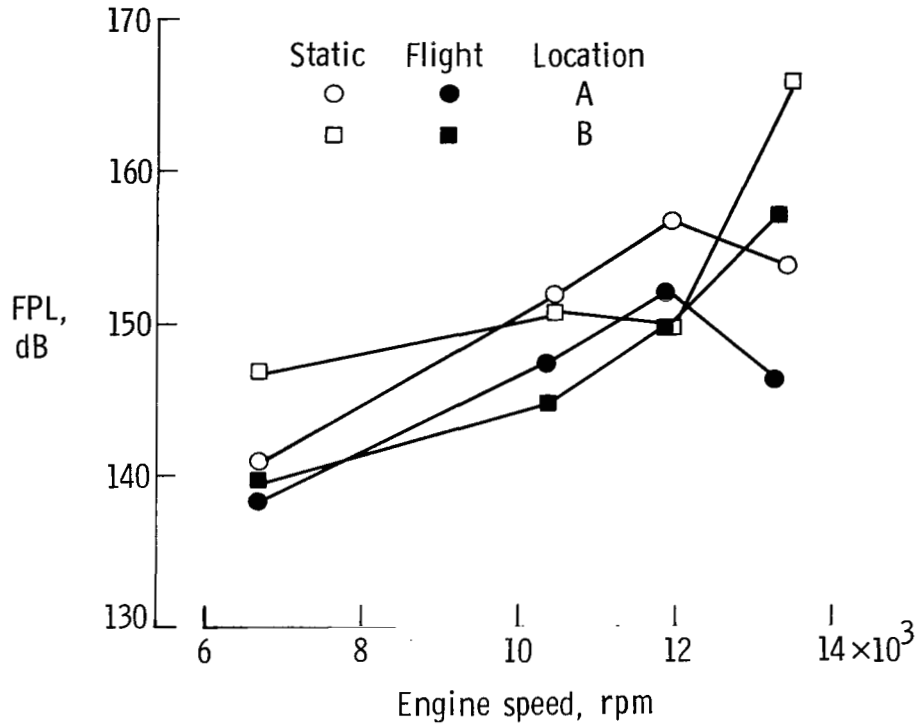
Figure 27.- Comparison of static and flight measured narrow-band (50 Hz) fluctuating pressure levels at fan-rotor F_1 tone for core-stator locations A and B.
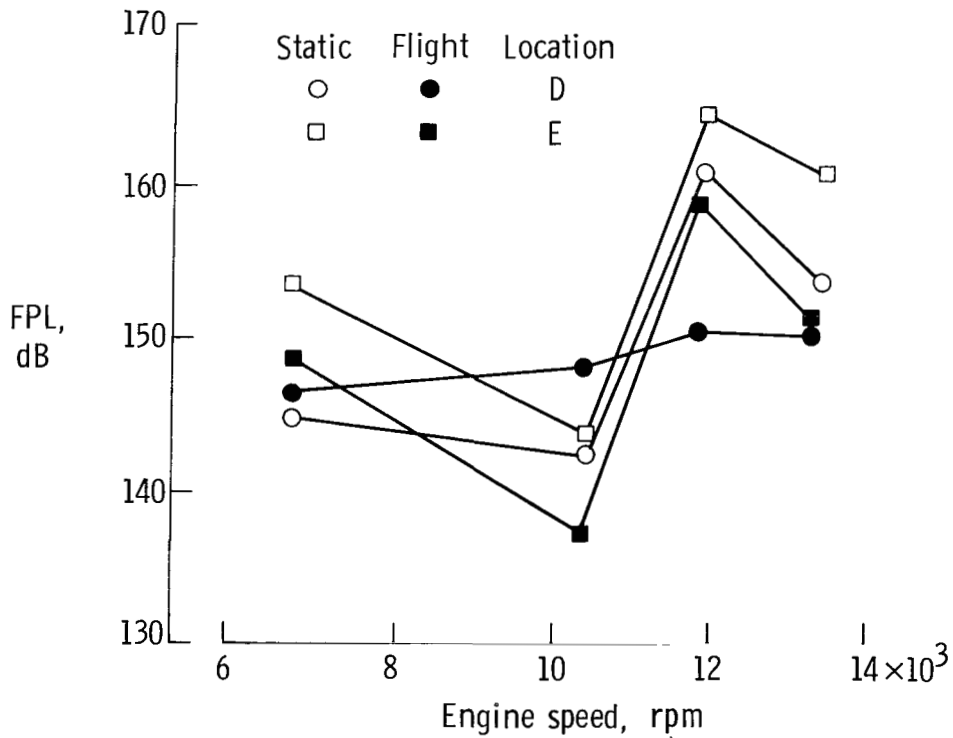
Figure 28.- Comparison of static and flight measured narrow-band (50 Hz) fluctuating pressure levels at fan-rotor F_1 tone for bypass-stator locations D an E.
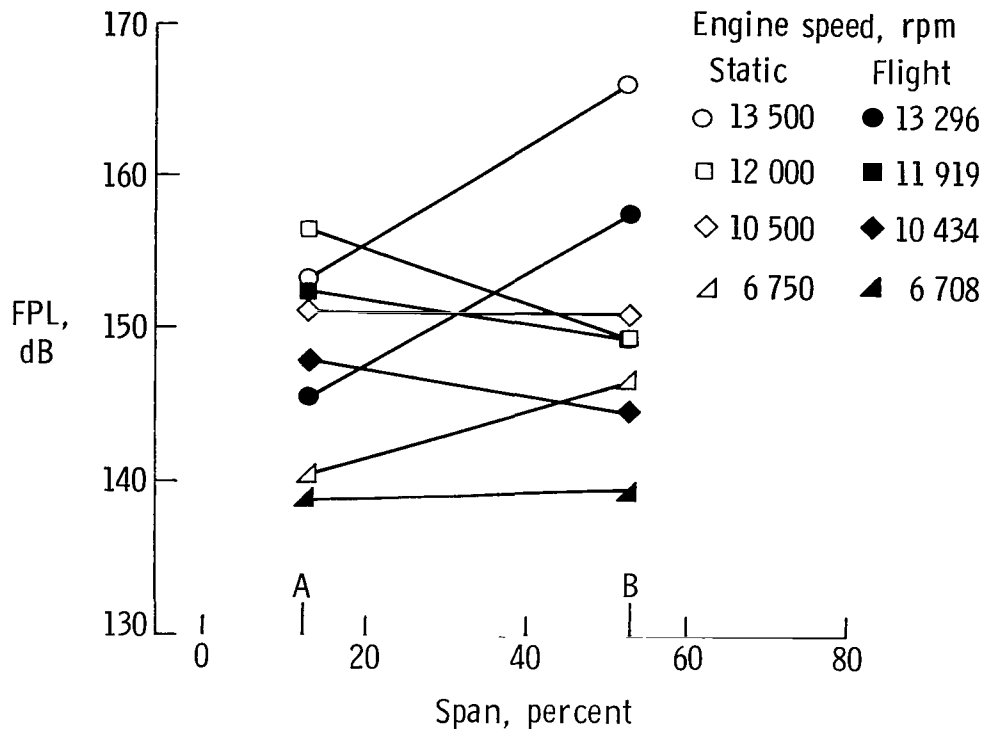
Figure 29.- Comparison of core-stator static and flight spanwise distribution of narrow-band (50 Hz) FPL of fan-rotor F_1 BPF tone.
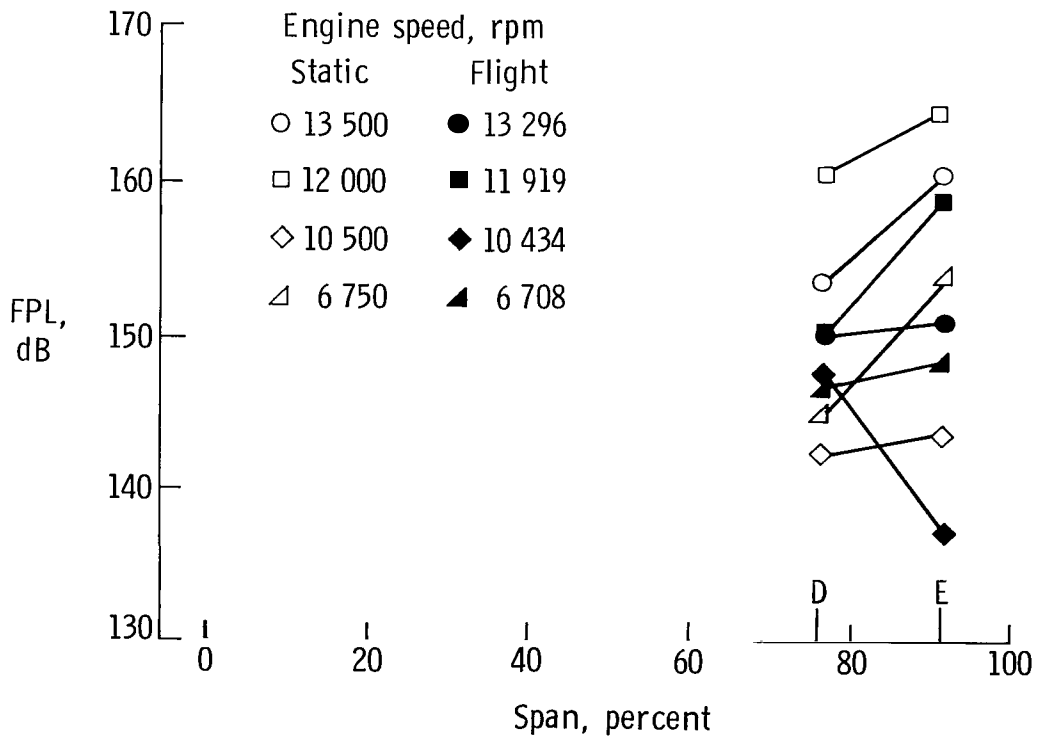
Figure 30.- Comparison of bypass-stator static and flight spanwise distribution of narrow-band (50 Hz) FPL of fan-rotor F_1 BPF tone.
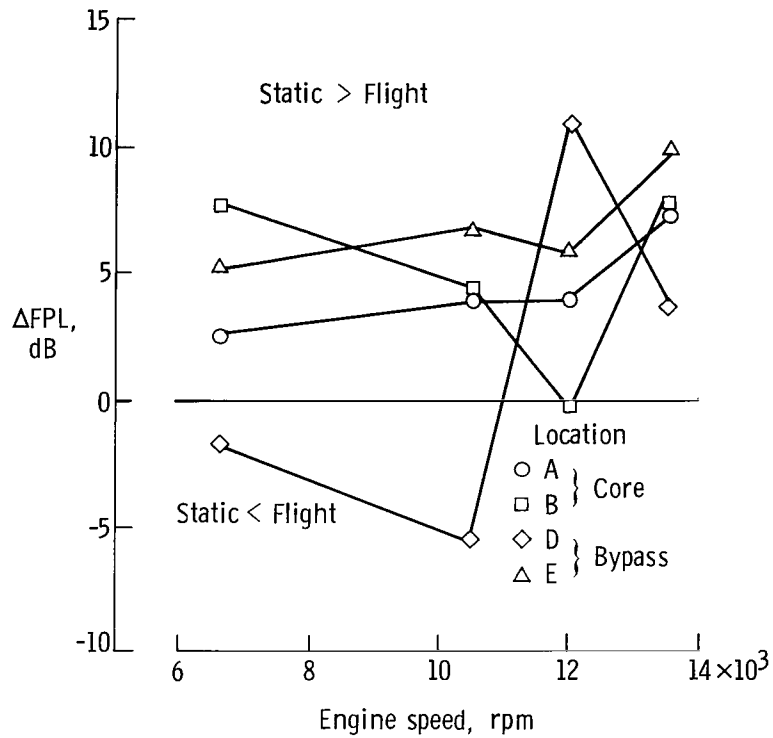
Figure 31.- Comparison of differences between static and flight
narrow-band (50 Hz) fluctuating pressure levels measured at
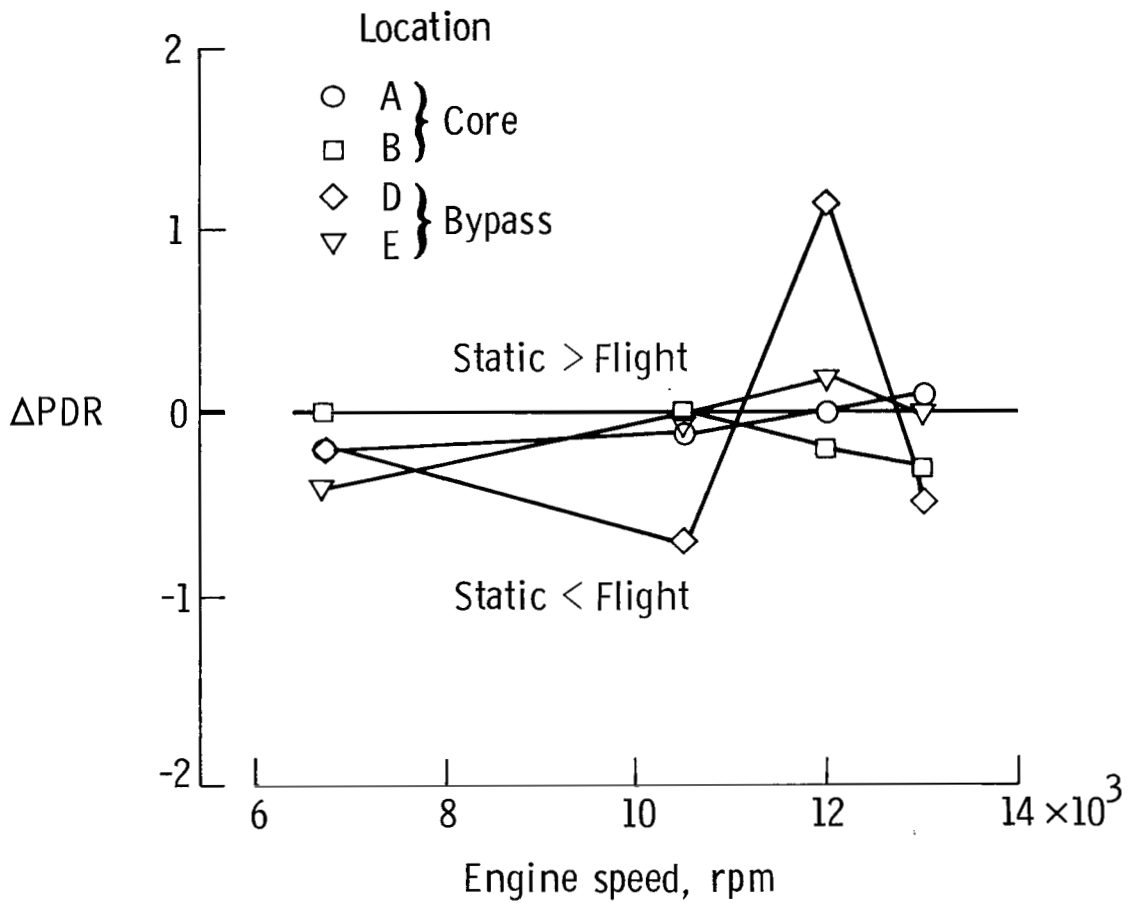stator locations for F_1 BPF tones at test engine speeds.
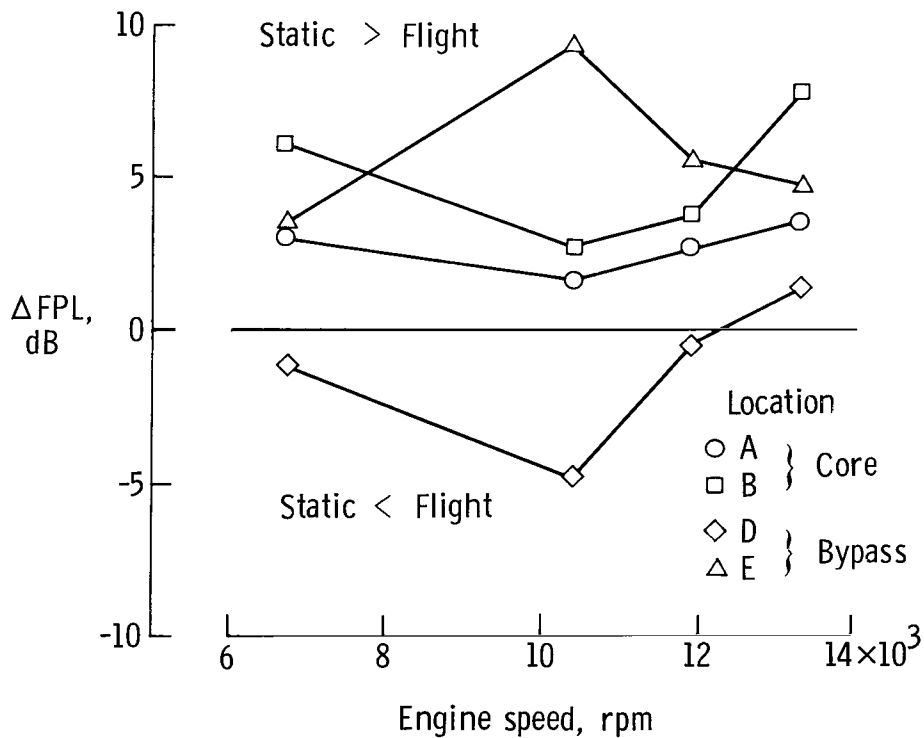
Figure 32.- Comparison of differences between static and flight
broadband fluctuating pressure levels measured at stator
locations for F_1 BPF tones at test engine speeds.

Figure 33.- Comparison of differences between static and flight probability density ratios of fluctuating pressures of F_1 BPF tones as measured at stator locations for test engine speeds.

National Aeronautics and
Space Administration

Washington, D.C.
20546

Official Business
Penalty for Private Use, $300

THIRD-CLASS BULK RATE

U.S.MAIL

```
1    1 1U,H,        840409 S00903DS
DEPT OF THE AIR FORCE
AF WEAPONS LABORATORY
ATTN: TECHNICAL LIBRARY (SUL)
KIRTLAND AFB NM 87116
```

NASA

POSTMASTER: If Undeliverable (Section 158
Postal Manual) Do Not Return

1. Report No. NASA TP-2217	2. Government Accession No.	3. Recipient's Catalog No.
4. Title and Subtitle STUDY OF STATOR-VANE FLUCTUATING PRESSURES IN A TURBOFAN ENGINE FOR STATIC AND FLIGHT TESTS		5. Report Date April 1984
		6. Performing Organization Code 505-31-33-13
7. Author(s) Arnold W. Mueller		8. Performing Organization Report No. L-15657
9. Performing Organization Name and Address NASA Langley Research Center Hampton, VA 23665		10. Work Unit No.
		11. Contract or Grant No.
12. Sponsoring Agency Name and Address National Aeronautics and Space Administration Washington, DC 20546		13. Type of Report and Period Covered Technical Paper
		14. Sponsoring Agency Code

15. Supplementary Notes

16. Abstract

As part of a program to study the fan noise generated from turbofan engines, fluctuating surface pressures induced by fan-rotor wakes were measured on core- and bypass-stator outlet guide vanes of a modified JT15D-1 engine. Tests were conducted with the engine operating on an outdoor test stand and in flight. The amplitudes of pressures measured at fan-rotor blade-passage fundamental frequencies were generally higher and appeared less stable for the static tests than for the flight tests. Fluctuating pressures measured at the blade-passage frequency of the high-speed core compressor were interpreted to be acoustic; however, disturbance trace velocities for either the convected rotor wakes or acoustic pressures were difficult to interpret because of the complex environment.

17. Key Words (Suggested by Author(s)) Turbofan noise source Stator-vane fluctuating pressures Static and flight noise tests Probability-density analysis Fan-rotor wakes	18. Distribution Statement Unclassified – Unlimited Subject Category 71		
19. Security Classif. (of this report) Unclassified	20. Security Classif. (of this page) Unclassified	21. No. of Pages 52	22. Price A04